5-8-2015

Impact of Ocean Acidification on Aphotic Biogeochemical Production of Reactive Oxygen Species

Sarah Ann Murphy
University of South Carolina - Columbia

Impact of Ocean Acidification on Aphotic Biogeochemical Production of Reactive Oxygen Species

By

Sarah Ann Murphy

Bachelor of Arts
Saint Mary's University of Minnesota, 2010

Master of Science
University of South Carolina, 2012

Submitted in Partial Fulfillment of the Requirements

For the Degree of Doctor of Philosophy in

Chemistry

College of Arts and Sciences

University of South Carolina

2015

Accepted by:

John L. Ferry, Major Professor

Timothy J. Shaw, Chairman, Examining Committee

Hans-Conrad zur Loye, Committee Member

David C. Volz, Committee Member

Lacy Ford, Vice Provost and Dean of Graduate Studies

Dedication

To Nik and my grandparents.

Abstract

Reactive oxygen species (ROS) are critical to global maintenance of the global organic carbon cycle, sulfur cycle, oxygen cycle, and transition metal cycles. The primary source of ROS is commonly considered to be photolysis or photochemically driven reactions, however ROS also exist in aphotic zones. A geochemical mechanism for the same in dark environments based on the tidally driven, episodic movement of anoxic groundwaters through oxidized, Fe(III) rich sediments is shown. Predictive models were developed based on *in vitro* experiments and tested using sediment samples collected from a saline tidal creek in the estuary at Murrell's Inlet, South Carolina. These sediments were air dried, resuspended in aerated solution, then exposed to aqueous sulfide at a range of concentrations chosen to replicate the conditions characteristic of a tidal cycle, beginning with low tide. No detectable ROS production occurred from this process in the dark until sulfide was added. Sulfide addition resulted in the rapid production of hydrogen peroxide. The mechanism of hydrogen peroxide production was tested using a simplified three factor representation of the system based on hydrogen sulfide, Fe(II) and Fe(III). We show that changes in marine pH associated with predicted ocean acidification are sufficient to quench hydrogen peroxide formation, potentially reducing it by an order of magnitude relative to current marine conditions (e.g. from 18.3×10^{-6} M to 2.01×10^{-6} M over the range of conditions studied).

Table of Contents

List of Tables

List of Figures

Chapter 1: Structure of the Manuscript

This dissertation is in manuscript style, structurally based on a literature review and journal entries published, submitted, or in process.

Chapter 2: A new perspective on global ROS production: aphotic mechanisms from biogeochemical sources

ABSTRACT

Reduced carbon and transition metals that coexist in the terrestrial biosphere lead to unpredicted high concentrations of reactive oxygen species (ROS), which are critical to maintenance of the global organic carbon cycle, sulfur cycle, oxygen cycle, and transition metal cycles. The primary source of ROS is commonly considered to be photolysis or photochemically driven reactions, however ROS also exist in aphotic zones. Here we show biogeochemical sources for superoxide, which can lead to the formation of other ROS. The contribution of sulfur to ROS production was calculated. This mini-review focuses on these aphotic mechanisms for ROS production, a key component of many elemental cycles.

INTRODUCTION

In most aquatic systems, photolytic reactions are limited to only a relatively thin surface layer through which light passes. In addition to indirect and direct photochemical reactions, aphotic mechanisms can produce significant concentrations of ROS, potentially surpassing photochemical processes in biogeochemically mediated aphotic systems. ROS production is often rapid, limited primarily by the presence of thermodynamically available reductants. Although the reaction between hydrogen sulfide and dissolved oxygen is spin forbidden, the oxidation of sulfide by dissolved oxygen is catalyzed by

dissolved metals, allowing fast oxidation of sulfide and production of ROS[1]. Additionally, a wide variety of bacteria produce superoxide directly[2].

Sulfide is widely available due to sulfate reduction in aqueous solutions, sediments, and biofilms by sulfate reducing bacteria. Two pathways have been proposed for the oxidation of sulfide in ROS and Fe containing systems: oxidation by hydroxyl radical (eqn 1-2) and 2 electron transfer via nanoparticles or clusters of FeS (eqn 3). Although both processes certainly occur to some extent, an increased net production of ROS in the presence of sulfide,[1] indicates the 2 electron transfer (eqn 3) is likely the dominate sulfide oxidation pathway resulting in a net increased concentration of ROS. The kinetically rapid oxidation of sulfide is enabled by Fe redox chemistry upon mass transport to oxic waters Environmental locations where this occurs include swamps, marshes and groundwater outlets, particularly where there is rapid mixing such as in coastal estuaries and beaches.

$$HS^- + HO\cdot \rightarrow HS\cdot + HO^- \quad (1) \quad [3]$$

$$HS\cdot + O_2 \rightarrow S^0 + O_2^- \quad (2) \quad [3]$$

$$HS^- + 2Fe(III) \rightleftarrows S^0 + 2Fe(II) \quad (3) \quad [3\text{-}5]$$

Although a variety of transition metals undergo similar processes[3], Fe is the most abundant and is a well-known producer of ROS through Fenton chemistry (eqn 4-5). This initiates a suite of reactions that convert superoxide to hydrogen peroxide and hydroxyl radical (eqn 6-8). The Fe cycle is completed by subsequent reduction of Fe(III) by reduced sulfur species (eqn 3). Although sulfide has the potential to donate up to 8 electrons to reduce Fe(III) and form superoxide, some oxidation states of sulfur may act

as a sink for ROS rather than a source (eqn 9). Additionally, particularly as pH decreases from modern day marine pH, other common molecules will compete as sinks for ROS (eqn 10).

$$Fe(III)L \xrightarrow{h\nu, LMCT} Fe(II)_{aq} + L_{ox} \quad (4)$$

$$Fe(II)_{aq} + O_2 \rightleftarrows Fe(III) + O_2^- \quad (5) \quad [6]$$

$$Fe(II) + HO_2\cdot \overset{H^+}{\rightleftarrows} H_2O_2 \quad (6) \quad [7]$$

$$2\ O_2^- / HO_2\cdot \overset{H^+}{\rightleftarrows} H_2O_2 + O_2 \quad (7) \quad [7]$$

$$M^{x+}_{aq} + H_2O_2 \rightleftarrows M^{(x+1)+} + HO\cdot + HO^- \quad (8) \quad [8]$$

$$H_2O_2 + HSO_3^- \rightarrow HSO_4^- + H_2O \quad (9) \quad [9]$$

$$HO\cdot + CO_3^{2-} \overset{H^+}{\rightarrow} CO_3^{-}\cdot + H_2O \quad (10) \quad [10]$$

There are many factors that directly influence the production of ROS, primarily dissolution, reduction and oxidation rates of Fe. The dissolution rate of Fe is increased by the presence of ligands such as carboxylic acids and sulfides[11-12]. Dissolution, reduction and oxidation rates are all strongly influenced by pH changes due to ocean pH approaching several critical pKa values, including carbonate (6.4) and sulfite (7.2).

As pH decreases, ROS scavenging by carbonate and sulfite will increase significantly. The rate of hydrogen peroxide scavenging by sulfite will increase by an order of magnitude with a change in pH from about 8.2 to 7.5[13]. As a global estimate, based on 11.3 teramoles of sulfate reduced annually[14], one order of magnitude change in the rate of bisulfite scavenging implies that up to 10 more teramoles of ROS may be scavenged by sulfite, rather than reduced carbon. Currently, 12-29% of the organic

carbon flux to the sea floor is dependent on the reduction of sulfate through metabolic activities[14]. The global absolute minimum input of geochemical aphotic ROS is 51 gigamoles of ROS based on net rate of loss of superoxide[15] and measured ROS concentrations in aphotic marine waters[16]. Because these samples were unaltered (net rate calculations include bacterial production and consumption of ROS, presumably also including indirect production of ROS through reduction of sulfates), the calculation of 51 gigamoles ROS defines the minimum contribution of mass transport and mixing of thermodynamically reactive chemical species to the marine ROS cycle. Additionally, tidal forcing promotes rapid mixing of reduced Fe and S with dissolved oxygen,[17] allowing rapid indirect sulfide oxidation by dissolved oxygen through Fe catalysis[18-20] or direct oxidation by Fe(III)[21]. The oxidation of sulfide results in the formation of S radicals, polysulfides, bisulfite, thiosulfate, and eventually sulfate.

In this mini-review, biogeochemical sources of ROS were discussed and global contributions were calculated. An overview of the positive and negative contributions (production and consumption, respectively) of sulfur to global ROS production is provided and the influence of pH on net production and consumption rates was briefly discussed. Additional work is needed to quantify aphotic changes as a function of pH[18, 22-27].

Chapter 3: Geochemical Production of Reactive Oxygen Species from Biogeochemically Reduced Fe[1]

*Sarah A. Murphy, Benson M. Solomon, Shengnan Meng, Justin M. Copeland, Timothy J. Shaw, John L. Ferry**

Department of Chemistry and Biochemistry, University of South Carolina, Columbia, South Carolina 29208, United States

KEYWORDS submarine groundwater, reactive membrane, remediation, transient oxidants

ABSTRACT

The photochemical reduction of Fe(III) complexes to Fe(II) is a well known initiation step for the production of reactive oxygen species (ROS) in sunlit waters. Here we show a geochemical mechanism for the same in dark environments based on the tidally driven, episodic movement of anoxic groundwaters through oxidized, Fe(III) rich sediments. Sediment samples were collected from the top 5 cm of sediment in a saline tidal creek in

[1] Sarah A. Murphy, Benson M. Solomon, Shengnan Meng, Justin M. Copeland, Timothy J. Shaw, and John L. Ferry. 2014. *Environmental Science and Technology*. 48 (7): 3815-3821.

the estuary at Murrell's Inlet, South Carolina and characterized with respect to total Fe, acid volatile sulfides and organic carbon content. These sediments were air dried, resuspended in aerated solution, then exposed to aqueous sulfide at a range of concentrations chosen to replicate the conditions characteristic of a tidal cycle, beginning with low tide. No detectable ROS production occurred from this process in the dark until sulfide was added. Sulfide addition resulted in the rapid production of hydrogen peroxide, with maximum concentrations of 3.85 micromolar. The mechanism of hydrogen peroxide production was tested using a simplified three factor representation of the system based on hydrogen sulfide, Fe(II) and Fe(III). The resulting predictive model for maximum hydrogen peroxide agreed with measured hydrogen peroxide in field-derived samples at the 95% level of confidence, although with a persistent negative bias suggesting a minor undiscovered peroxide source in sediments.

INTRODUCTION

The cycling of Fe between ferrous and ferric oxidation states constitutes a catalytic mechanism of electron transport in aqueous environments ranging from sediments to surface waters.[1-3, 28] This cycle is coupled to atmospheric oxygen through the reduction of O_2 by ferrous iron. In the photic zone, ferrous iron formation is generally photoinduced through the photolysis of Fe(III)-ligand (L) complexes, particularly when L = carboxylic acids (eqn 3.1).[29-31] The resultant $Fe(II)_{aq}$ is thermodynamically unstable in the presence of dissolved oxygen and its oxidation leads to the production of the superoxide anion radical (eqn 3.2). The superoxide anion radical is the conjugate base of the hydroperoxyl radical (pKa 4.8). This radical can react with a second $Fe(II)_{aq}$ or disproportionate to generate hydrogen peroxide (eqns 3.3, 3.4).[32-34] Hydrogen peroxide in turn can react with

reduced transition metals (M^{x+}) to yield the hydroxyl radical (eqn 3.5).[35-36] In sediments, aquifers, and anoxic porewaters microbial respiration can replace photons as the source of reductive equivalents to drive $Fe(II)_{aq}$ production. This is accomplished through a combination of direct microbial reduction and indirect reduction by microbially produced agents such as hydrogen sulfide (eqn 3.6).[37-38] Reduced sulfur species, derived from anaerobic microbial reduction of sulfate, can occur in groundwaters at concentrations as high as millimolar.[39]

Reaction	**Eqn #**	**Ref. #**
$Fe(III)L \xrightarrow{h\nu, LMCT} Fe(II)_{aq} + L_{ox}$	(3.1)	
$Fe(II)_{aq} + O_2 \rightleftarrows Fe(III) + O_2^{-}\cdot$	(3.2)	6
$Fe(II) + HO_2\cdot \underset{\rightleftarrows}{H^+} H_2O_2$	(3.3)	7
$O_2\cdot + HO_2\cdot \underset{\rightleftarrows}{H^+} H_2O_2 + O_2$	(3.4)	7
$M^{x+}_{aq} + H_2O_2 \rightleftarrows M^{(x+1)+} + HO\cdot + HO^-$	(3.5)	8
$Fe(III) + HS^- \rightleftarrows Fe(II)_{aq} + HS\cdot$	(3.6)	21

Reactions 1-5 suggest microbially generated $Fe(II)_{aq}$ can have the same impact on ROS production as photochemical sources of ROS, but with magnitude mediated by mass transport rather than light intensity.[3, 40-41] Major sources of $Fe(II)_{aq}$ and hydrogen sulfide-rich waters include the outflow of subterranean estuaries,[42] the release of sediment-associated porewater during low tide,[43] mine drainage[44] and the emissions of some hydrothermal vents.[4] Subterranean estuaries and tidally driven mixing are particularly significant among these sources because their releases are in close proximity to high human population densities near coastal regions.[45-47] Recent studies indicate the volume of

groundwater associated with subterranean estuary emission represents a major, continuous flux of $Fe(II)_{aq}$ to the groundwater/seawater mixing zone.[48-50] Estimates based on Ra isotope inventories suggest that on the order of 30 kg water $m^{-2}day^{-1}$ is circulated through the shallow aquifer in the South Carolina salt marsh system alone.[51] This yields an estimate for the entire South Carolina coastline (est. 2000 km^2 salt marsh) of approximately 6.0 $x10^{10}$ kg of water exchanged between the oxic and anoxic conditions per day.[52] The implication is this ecosystem has a potential daily abiotic ROS flux of up to 1.5 $x10^7$ moles day^{-1} (based on the accompanying dissolved oxygen flux). This number is comparable to photochemical sources of ROS, based on measured steady state concentrations of reactive oxygen species in near shore environments.[32, 53-54] These numbers are rough estimates yet still suggest an important hypothesis: the number of moles of reactive oxygen species derived from $Fe(II)_{aq}$ rich groundwater is potentially on par with that obtained from photochemical processes, with biogeochemical reductants (e.g. sulfide) acting as initiators in a manner analogous to photons.

Direct measurement of the ROS production capacity of a given environmental compartment is a difficult challenge because of the transient nature of the analytes involved. There is a long tradition in aqueous ROS chemistry of addressing that problem by removing a representative fraction of the system in question from the field and initiating ROS production in a laboratory setting.[31, 55-56] This work reports application of that strategy to test the hypothesis expressed in the preceding paragraph. This was done by infusing oxic sediment samples from a protected coastal marsh with sulfidic solutions (the initiation step) and monitoring subsequent ROS formation. Sediment samples were obtained from the surface of a pristine saline tidal creek at low tide (i.e. top five cm of exposed creek

bottom, flooded with seawater at high tide, pH 8.0, salinity of 28 ppt). Varying concentrations of hydrogen sulfide were spiked into sediments and hydrogen peroxide generation was measured as a function of added sulfide and time. The duration of peroxide generation increased with increasing sulfide but the maximum concentration was constant, consistent with catalytic Fe oxidation/reduction cycles that continued until the sulfide was depleted. The mechanism of peroxide production was tested by comparing these outcomes to those obtained from a trifactorial experiment based on the cooxidation of $Fe(II)_{aq}$ and sulfide in solution in the presence of Fe(III) (central composite design, 15 conditions interrogated, *vide infra*).

EXPERIMENTAL METHODS

Materials: Iron(III) chloride hexahydrate and sodium sulfide nonahydrate (99.99+% trace metal free) were purchased from Aldrich. Hydrochloric acid (ACS grade) was obtained from BDH. *N*,*N*-dimethyl-p-phenylenediamine sulfate salt was acquired from Acros Organics. Diethylenetriaminepentaacetic acid (98+%) and iron(II) chloride anhydrous (99.5+%) were purchased from Alfa Aesar. Iron(II) chloride was stored in a desiccator. FerroZine iron reagent (98%) was purchased from VWR. All other salts (99%) were obtained from Fisher Scientific. All chemicals were used as received. Solutions were made in Barnstead E-pure (18 MΩ cm^{-1}) water which had been distilled under nitrogen to remove trace H_2O_2.

ANALYTICAL METHODS

Iron(II) and Sulfide Measurement. $Fe(II)_{aq}$ and hydrogen sulfide were monitored colorimetrically using the ferrozine and methylene blue methods respectively.[57-60] Samples

were withdrawn from the reactor and added directly to developing solutions (varied by analyte). Absorption spectra were recorded on a Spectramax M5 plate reader.

Hydrogen Peroxide. Hydrogen peroxide was measured by the acridinium ester chemiluminescence technique utilizing a flow injection analysis instrument with a chemiluminescence detector (Waterville Analytical, Waterville, ME).[61-62] Chemiluminescence from the reaction between the hydroperoxyl anion and acridinium ester at pH 11.4 was monitored in a flow through cell by a photon multiplier (PMT). All initial flow rates (sample, carrier, acridinium ester, and buffer) were set at a constant 1.5 mL/min. The flow cell volume was 2 mL, with a PMT integration time of 0.200 s and a constant voltage for every experiment set. Daily calibration was achieved by the use of independently verified (UV absorbance at 2.54 $x10^{-7}$ m) peroxide solutions, with hourly drift checks based on standard comparison. New calibrations were performed at least twice/measurement period or when instrument drift exceeded 10%.

All glassware used was cleaned in a muffle furnace and acid washed. After rinsing with 18MΩ deionized water, glassware was handled and stored as trace metal clean glassware to prevent trace metal catalytic oxidation of sulfide in the absence of added metals.

Sediment Experiments. Sediment samples were collected from a tidal creek (Bread and Butter Creek) in North Inlet, part of the Baruch Institute reserve near the town of Murrell's Inlet, South Carolina (Figure 3.14). Collected sediments included both oxic and anoxic layers. Anoxic portions were sulfidic with a loading of 26.5µmol/g acid volatile sulfides based on dry weight. Aqueous sediment loading was 10.00 g L^{-1} of air dried, sieved sediment, consistent with the low range of solid/liquid ratio (99% porosity) observed

in the top layers of many coastal surface sediments.[63] Sediments were stirred for 20 minutes prior to the addition of sulfide and buffered to pH 8.28 with $NaHCO_3$ (0.050 M). Samples were removed from the reactors and spun down on a Baxter Dade Immufuge II centrifuge at 3225 rpm for 30 seconds to remove suspended solids before subsequent spectroscopic assays.

Quality Assurance/Quality Control. Replicate blanks (*n=3*) were obtained for all reagents. Blanks were updated with preparation of fresh reagent solutions. Reference standards were interrogated for peroxide analysis at a frequency of 1 reference check/5 unknown determinations. Peroxide reference standards were externally calibrated against their optical absorbance at 254 nm. The detection limit for each method was defined by the linear dynamic range of the calibration curves.

EXPERIMENTAL DESIGN

The multifactorial experiments were designed to interrogate the relationship between peroxide yield and the initial concentrations of $Fe(II)_{aq}$, total Fe(III), and hydrogen sulfide. Specific conditions for each experiment were determined by processing the conditional ranges for each variable through the central composite design algorithm, which solved for specific points in parameter space that required experimentation. This design was chosen to allow an estimate of feedback terms, a necessary experimental component for systems based on free radical reactions that may involve self-disproportionation in the final observables. This method of interrogation allowed development of models based on the correlation of experimental outcomes with initial conditions without exhaustive understanding of the fundamental equilibria and kinetic constants for every step of the system.

The concentration ranges for each factor were chosen based on reported field measurements to ensure environmental relevance.[39, 64-66] Similar models have previously been shown competent for accurately predicting net oxidation rates in complex multistep reaction systems.[59-60, 67]

The pH of each reaction was monitored to ensure consistency. A pH probe (Cole Palmer pH electrode, general purpose, combination, refillable, glass body, BNC) was calibrated at the appropriate ionic strength condition and used to monitor pH throughout. Mean pH for the experimental array was = 8.28 ± 0.07 reported as one standard deviation. The ionic strength of the solutions was established by the buffer; the sum of all other ionic species added contributed less than 2% to the total. All measurements were performed in triplicate, except the midpoint (initial conditions 1.50 $x10^{-4}$ M $Fe(II)_{aq}$, 1.50 $x10^{-4}$ M Fe(III), and 2.50 $x10^{-4}$ M HS^-), which was performed n = 6 times. The experimental sequence was randomized to eliminate time dependent artifacts. All experiments were conducted in a dark room to minimize photochemical reactions. The correlation between pH variability and measured outcomes (Figure 3.62, Figure 3.63) was less than 0.1, indicating pH was not a statistically significant factor across the experimental design.

RESULTS

The multifactorial experiments were justified based on the hypothesis that complex sediment samples could be reductively modeled as equivalent to mixtures of aqueous solutions of Fe(II), HS^- and Fe(III) as they came to thermodynamic equilibrium with dissolved oxygen. Air saturated solutions of HS^- were stable at pH 8.28 in the presence and absence of added hydrogen peroxide (Figure 3.71). Separate Fe(III) solutions and hydrogen sulfide solutions were monitored over time and no hydrogen peroxide evolution

was detected. However the joint addition of Fe(II) and Fe(III) to oxic HS^- solutions resulted in the oxidation of Fe(II) and HS^- along with the initial rapid reduction of some Fe(III) (Figure 3.1). The ratio of the first derivatives of [HS^-] and [Fe(II)] plotted vs time approached unity after the initial Fe(III) reduction phase, indicating the catalytic function of Fe(II) in enabling the oxidation of HS^- by O_2 (Figure 3.1 inset).

The evolution of hydrogen peroxide was monitored under all conditions of the trivariate experiment and observed to range from a minimum below the detection limit and a maximum of 2.3 $x10^{-5}$ M (Figure 3.2). An ANOVA table was constructed to determine the relationship between the hydrogen peroxide and the initial concentrations of Fe(II), HS^- and Fe(III). The maximum concentration of hydrogen peroxide for each experimental condition was correlated against all three individual factors, their squared terms (curvature) and the possible interactions in accordance with the quadratic fit of the central composite design algorithm (Table 3.2). The factors could be fit to the maximum hydrogen peroxide yield with an unadjusted R^2 of 0.919. The model was constructed assuming each term (x) had a coefficient, β_x. The statistical significance of each term to the outcome was determined by applying the t-test to the hypothesis that $\beta_x \neq 0$ at the 95% level of confidence. Factors with β_x values that did not test as significantly different from 0 were statistically and practically unimportant to hydrogen peroxide. $[Fe(II)]_{aq}$, $[HS^-]$, $[Fe(II)]_{aq}^2$, $[HS^-]^2$ and the $[Fe(II)]_{aq}$-$[HS^-]$ interaction terms were significant to the outcome at the 95% level of confidence. The sign on the associated β_x values indicated the direction of contribution of that factor to the model outcome. Elimination of the remaining terms yielded an adjusted R^2 of 0.899. When their corresponding uncoded β_x terms and the

intercept (Table 3.2) were included, the resulting empirical model for predicting the maximum concentration of hydrogen peroxide was (eqn 3.7):

$$[H_2O_2]_{max}^{1/2} = -0.3064 + 1.673\,x10^{-2}\left([Fe(II)]_{aq}x10^{6}\right) + 1.305x10^{-2}([HS^{-}]x10^{6}) + 2.243x10^{-5}\left([Fe(II)]_{aq}x10^{6}\right)([HS^{-}]x10^{6}) - 4.325x10^{-5}\left([Fe(II)]_{aq}x10^{6}\right)^{2} - 2.529x10^{-5}([HS^{-}]x10^{6})^{2} \quad (3.7)$$

A sum of squares value was obtained from the ANOVA table for the model and each factor (Table 3.5). The ratio of the value for each factor over the value for the model provided a rough estimate of the percent impact attributable to that factor on the maximum yield of hydrogen peroxide (Table 3.2).

A series of field-derived sediment samples were characterized (*vide supra*) and suspended in aerated solution of hydrogen sulfide and equilibrated with oxygen. The measured initial values of Fe(II) and HS^- were then entered into the model (eqn 3.7) to generate predicted H_2O_2 maxima. The validity of the initial hypothesis was tested by comparison between the measured and predicted hydrogen peroxide maxima at the 95% level of confidence.

Equilibration experiments were conducted with aqueous suspensions of tidal creek sediment (Bread and Butter Creek Figure 3.14), 1.00 wt % suspension; composition 21% C, 2% N, 1.2% total Fe). Sediments were aerated in the dark in the absence or presence of added hydrogen sulfide. Samples removed prior to sulfide addition contained detectable amounts of Fe(II) (detection limit of 2.0 $x10^{-6}$ M, whereas $[HS^-]$ and $[H_2O_2]$ were both

below their respective detection limits (3.0 ±1.5 $x10^{-6}$ M and 2.50 ±0.90 $x10^{-7}$ M, Figure 3.74). Native Fe(II) sources in the samples contributed to an Fe(II) background of 9.1±2.9 $x10^{-6}$ M. Additional suspensions were prepared and sufficient hydrogen sulfide added to raise the nominal initial concentration to 3.00 $x10^{-4}$ M (Figure 3.3) or 6.00 $x10^{-4}$ M (Figure 3.4). These conditions were chosen to emulate tidally driven measured groundwater exchange (the outward pulse) through sediments.[14, 50-55] Dissolved O_2 reduction in the latter suspensions was rapid with concurrent oxidation of hydrogen sulfide and formation of $Fe(II)_{aq}$ (Figure 3.3 and 3.4). $Fe(II)_{aq}$ fell to pre-sulfide spike concentrations after added hydrogen sulfide was consumed, in agreement with existing models of Fe-catalyzed O_2 driven oxidation (e.g. the Udenfriend reaction and many subsequent works) and the results of the trivariate model. [38, 74-78] Subsequent additions of hydrogen sulfide to the sediment suspensions resulted in essentially identical reactant/product production and consumption profiles (Figures 3.68-3.70) as long as oxygen concentrations were maintained. $Fe(II)_{aq}$ never reached the concentration that would be predicted from the reductive equivalents added (as hydrogen sulfide), presumably due to its simultaneous oxidation by dissolved oxygen (eqs 3.2, 3.6). Hydrogen peroxide concentration increased as sulfide concentrations fell to near the detection limit, approaching a maximum of 3.85 and 2.83 $x10^{-6}$ M for 300 and 6.00 $x10^{-4}$ M hydrogen sulfide added respectively (Figures 3.3 and 3.4). $Fe(II)_{aq}$ achieved a maximum concentration within 30 s and maintained at a pseudo-stationary state until $[HS^-] < [Fe(II)]_{aq}$, then fell.

DISCUSSION

Aqueous solutions of ferrous and ferric iron, dissolved oxygen and hydrogen sulfide are a thermodynamically unstable mixture that occurs frequently if transiently in natural

waters as a result of mass trasport. They are associated with the movement of aqueous solutions across sharp redox gradients, particularly those imposed by microbial consumption of oxygen or the action of sulfate reducers. Examples include the tidally driven release of submarine groundwater across the sediment-water column interface; the seasonal overturn of hypolimnetic waters, redox zonation in biofilms and other events corresponding to a large range of flow regimes.[79-86] They equilibrate rapidly on mixing with concurrent oxidation of reduced iron and production of superoxide. The corresponding rate of O_2 reduction is controlled by several variables, including the rate of precipitation of resulting Fe(III) or Fe(III)-L in the studied system. Under the conditions of this study (pH 8.28, 5.0 x10^{-2} M total CO_3^{2-} species, $[Fe(II)]_o$ < 3.00 x10^{-4} M) net Fe(II) oxidation in the absence of sulfide was expected to be quite rapid with an Fe(II) lifetime of less than 10 s.[59-60] Based on this assumption and eqn 3.1-3.5 the appearance of superoxide and H_2O_2 should have mirrored the rapid loss of Fe(II). However, previous work has shown sulfide capable of rapidly reducing $Fe(III)_{aq}$ to Fe(II).[77-78] In this study sulfide addition resulted in a net apparent decrease in Fe(II) oxidation rates, with ROS formation coupled to sulfide oxidation and Fe(II) oxidation as a result (as distinguished from previous work reporting ROS formation as a result of Fe(II) oxidation alone).[37, 59, 60, 67] The observation is supported by the results from the multifactorial experiment (Table 3.2) that indicate HS^- and FeS combined account for nearly 50% of the maximum hydrogen peroxide. Given that the direct reaction of HS^- with O_2 is spin forbidden this large positive impact indicates the intermediacy of Fe(II) as an electron shuttle between reduced S species and O_2 in the system. The relatively minor impact of FeS indicates that the reduction of Fe(III) by sulfide to produce Fe(II) was a more important source of reductive equivalents

in the studied system than the direct oxidation of FeS. Given that the oxidation of Fe(II) and FeS both yield superoxide, comparison of the FeS and Fe(II) terms also suggested that the reduction of superoxide by Fe(II) (eqn 3.3) was a more significant source for H_2O_2 than disproportionation.[87-88] However, changes in environmental conditions such as those associated with ocean acidification are likely to change the mechanism of H_2O_2 production, probably increasing the relative importance of dismutation if conditions are closer to pH 7.

The lack of significance of Fe(III) to maximum [H_2O_2] (as indicated by analysis of the model in Table 3.2) supported commutability of the solution-phase model to experiments containing natural sediments. Comparison of predicted H_2O_2 maxima from eqn 7 to the outcome of experiments measuring the equilibration of sediments with air; post-sulfide addition, showed close agreement between the two sets of experiments (Table 3.3). It was particularly notable that doubling the initial HS^- loading had no statistically significant effect on the maximum H_2O_2 yield. This suggested the family of associated reactions had reached a steady state limited by a factor independent of added sulfide, speculatively the rate of FeS oxidation. Although FeS is stable in oxic solution on the timescale of days, freshly prepared (amorphous) FeS is known to oxidize on the timescale of seconds to minutes, depending on solution conditions. The appearance of a steady state was consistent with the self-reactions of ROS that limit their concentrations and with the observation of negative β_x for the significant squared factors (Table 3.2).

It was notable that the sediments in this study had very a high concentration of organic carbon, approximately 20% by mass. This carbon was not deliberately extracted or modified during the experimental procedure and therefore was presumably a faithful representation of organic carbon in the field environment. Despite the large excess of

organic C in the suspensions eqn 7 predicted the outcome of both HS^- spike concentrations to within the 90% confidence interval; and to within the 95% confidence interval for the 3.00 $x10^{-4}$ M HS^- spike, although both sets of predictions were biased slightly low (Table 3.3). The low bias in eqn 3.7 could have also been a result of H_2O_2 produced during the peroxidation of organic C post-oxidation by HO•, but the bias was so small organic C was probably not a significant contributor to the H_2O_2 maximum. The high concentration of natural organic materials in the studied system indicated they were certainly the primary sink for secondary ROS such as HO• generated during the process yet they did not affect its outcome. These observations have significant implications for micropollutant fate and carbon cycling and suggest an abiotic link between microbial metabolism and carbon oxidation. If the partial oxidation of refractory carbon or other electron donors/acceptors through sulfide driven ROS production leads to modifications making them better microbial energy sources, this suggests an alternative pathway for microbial alteration and consumption of natural and anthropogenic organic carbon.[42, 89-90]

Table 3.1. Factor Concentration Range Subdivisions: Experimental factors and initial concentrations corresponding to the ranges chosen for the trivariate experiment.					
Coded value for each factor:					
β	-2	-1	0	1	2
Uncoded value for each factor (i.e. initial molar concentration):					
$[Fe(II)]_{aq}$ $x10^{-6}$ M	0	61	150	239	300
[Fe(III)] $x10^{-6}$ M	0	61	150	239	300
$[HS^-]$ $x10^{-6}$ M	0	101	250	399	500

Table 3.2. Uncoded coefficients (β_x) obtained by modeling the maximum H_2O_2 yield as a function of initial [Fe(II)], [Fe(III)] and $[HS^-]$. (R^2_{model} = 0.919; $R^2_{adjusted}$ = 0.899)				
β_x	Value	Sum of Squares	Estimated % contribution	p-value
$\beta_{0\ (intercept)}$	-0.3064	57.69		<0.0001
$\beta_{Fe(II)}$	$1.673\ x10^{-2}$	20.16	34.9	<0.0001
$\beta_{Fe(III)}$	NS[a]	0.08	NS[a]	0.4523
β_{HS-}	$1.305\ x10^{-2}$	23.10	40.0	<0.0001
$\beta_{Fe(II)Fe(III)}$	NS[a]	0.15	NS[a]	0.2948
$\beta_{Fe(II)HS-}$	$2.243\ x10^{-5}$	2.12	3.7	0.0003
$\beta_{HS-Fe(III)}$	NS[a]	0.31	NS[a]	0.1382
$\beta_{(Fe(II))2}$	$-4.325\ x10^{-5}$	3.29	5.7	<0.0001
$\beta_{Fe(III))2}$	NS[a]	0.00	NS[a]	0.9745
$\beta_{(HS-)2}$	$-2.529\ x10^{-5}$	8.68	15.0	<0.0001

[a] NS indicates "not significant" at the 95% level of confidence.

Table 3.3: Comparision of Sediment Experimental Hydrogen Peroxide Data to Model Predictions				
$[HS^-]$ initial	$[Fe(II)]_{aq}$ initial	[Fe(III)] initial	Sediment Data	Model Prediction
3.00×10^{-4} M	7×10^{-6} M	2.2×10^{-3} M	$3 \pm 1.8 \times 10^{-6}$ M	$2 \pm 0.9 \times 10^{-6}$ M
6.00×10^{-4} M	7×10^{-6} M	2.2×10^{-3} M	$4 \pm 1.8 \times 10^{-6}$ M	$2 \pm 0.9 \times 10^{-6}$ M

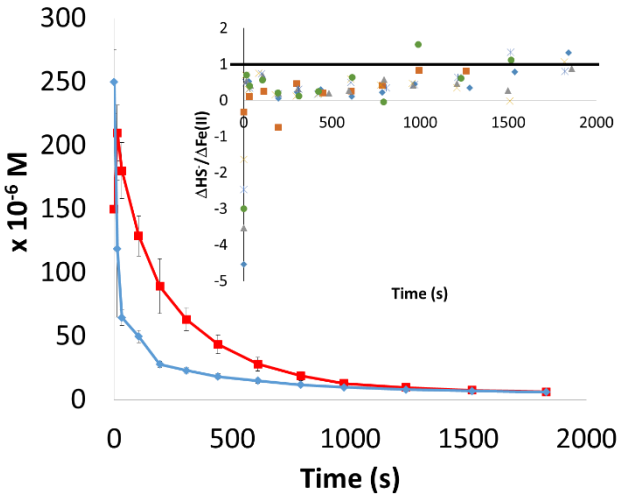

Figure 3.1. The concentration of (■) $Fe(II)_{aq}$ and (●) $[HS^-]$ during the oxidation of 1.50×10^{-4} M initial $Fe(II)_{aq}$ and 2.50×10^{-4} M initial hydrogen sulfide in the presence of 1.50×10^{-4} M initial Fe(III) is shown. Error bars shown are ±1 standard deviation based on n = 6 experiments. Inset: the ratio of the first derivatives of $[HS^-]$ and [Fe(II)], with a thick solid line to illustrate the approach to unity, six replicates shown.

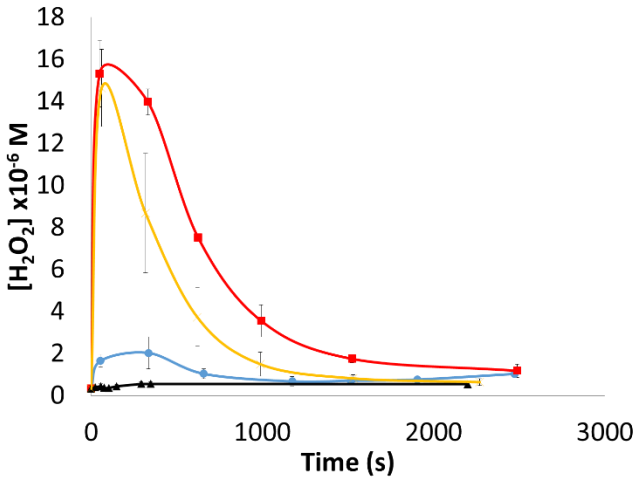

Figure 3.2. The concentration of peroxide with time. Initial conditions: (■), 1.50 x10^{-4} M $Fe(II)_{aq}$, 2.50 x10^{-4} M HS^-; (×) 1.50 x10^{-4} M $Fe(II)_{aq}$, 1.50 x10^{-4} M Fe(III), 2.50 x10^{-4} M HS^-; (●) 1.50 x10^{-4} M Fe(III), 2.50 x10^{-4} M HS^-; (▲) 1.50 x10^{-4} M $Fe(II)_{aq}$, 1.50 x10^{-4} M Fe(III). Error bars shown are ±1 standard deviation based on n = 3 experiments.

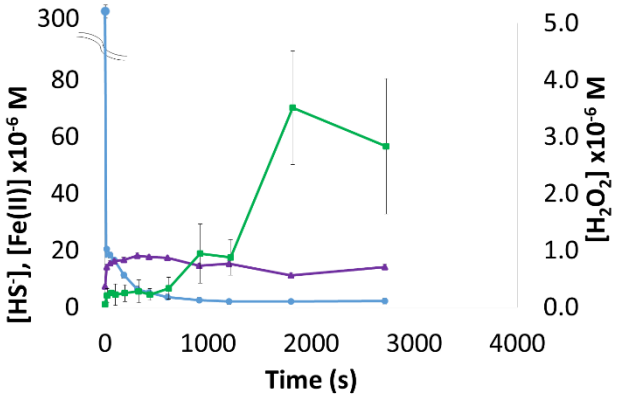

Figure 3.3. Concentration of (●) hydrogen sulfide, (▲) $Fe(II)_{aq}$, and (■) H_2O_2 during the injection of 3.00 x10^{-4} M hydrogen sulfide into a slurry of Bread and Butter Creek sediment (10.00 g sediment/L). Error bars are ±1 standard deviation based on n = 3 experiments.

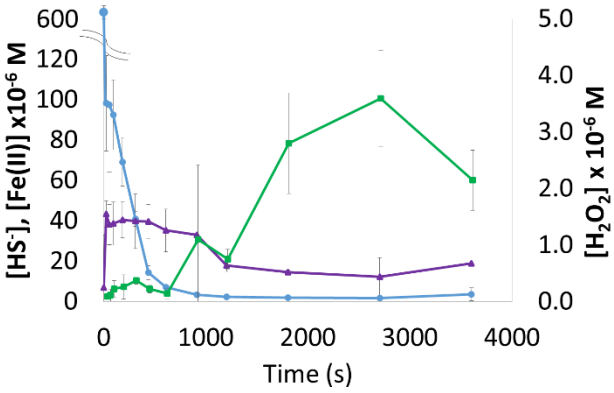

Figure 3.4. Concentration of (●) hydrogen sulfide, (▲) $Fe(II)_{aq}$, and (■) H_2O_2 during the injection of 6.00 $x10^{-4}$ M hydrogen sulfide into a slurry of Bread and Butter Creek sediment (10.00 g sediment/L) are shown. Error bars shown are ±1 standard deviation based on n = 3 experiments.

ASSOCIATED CONTENT

AUTHOR INFORMATION

Corresponding Author

*ferry@sc.edu; phone: 803-777-2646; fax: 803-777-9521.

Author Contributions

The manuscript was written through contributions of all authors. All authors have given approval to the final version of the manuscript.

Funding Sources

This work was supported by the U.S. National Science Foundation, Grant CHE-1308801.

Notes

The authors declare no competing financial interest.

ACKNOWLEDGMENT

The authors would like to extend special thanks to Kate Washburn and Prof. Tom Chandler for generously providing the Bread and Butter Creek sediment samples, Dr. Lijian He for AVS analysis, and to Joy Ihekweazu for help in the laboratory. We are also grateful to the reviewers for their work helping make a better paper.

SUPPORTING INFORMATION

Preliminary work, all $[Fe(II)]_{aq}$, $[HS^-]$, and $[H_2O_2]$ data, matrix outcomes, quality assurance/quality control data re pH, run order, etc; and peroxide consumption experiments can be found in Supporting Information. This material is available free of charge via the Internet at http://pubs.acs.org. In this publication, supporting information follows immediately.

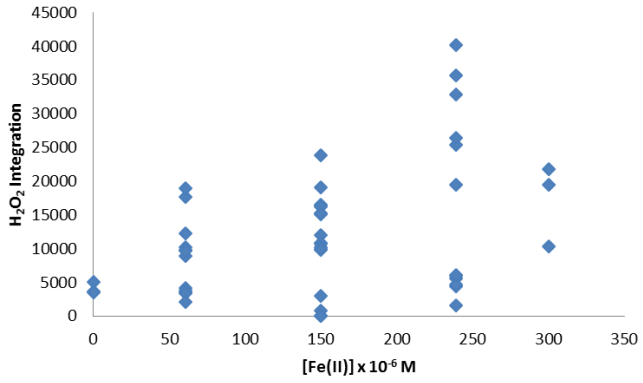

Figure 3.5. Hydrogen peroxide integration plotted against Fe(II) concentration. All matrix runs are represented by a unique point.

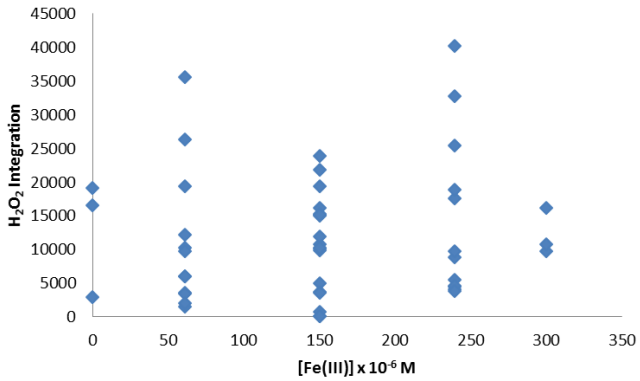

Figure 3.6. Hydrogen peroxide integration plotted against Fe(III) concentration. All matrix runs are represented by a unique point.

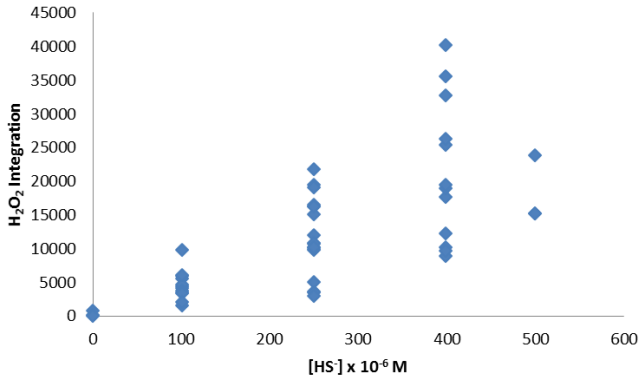

Figure 3.7. Hydrogen peroxide integration plotted against hydrogen sulfide concentration. All matrix runs are represented by a unique point.

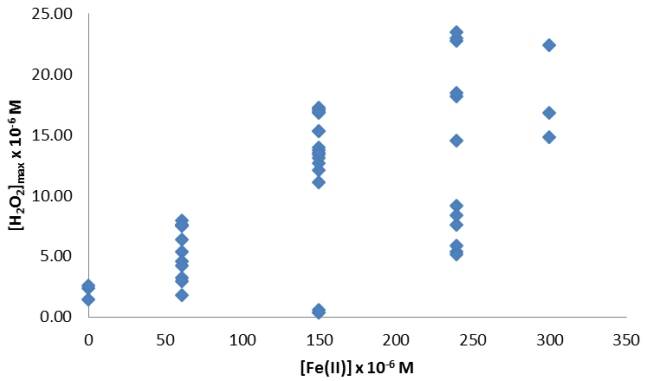

Figure 3.8. Hydrogen peroxide maximum concentration measured plotted against Fe(II) concentration. All matrix runs are represented by a unique point.

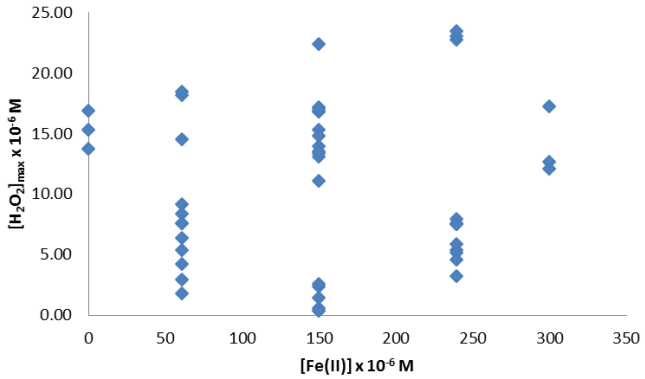

Figure 3.9. Hydrogen peroxide maximum concentration measured plotted against Fe(III) concentration. All matrix runs are represented by a unique point.

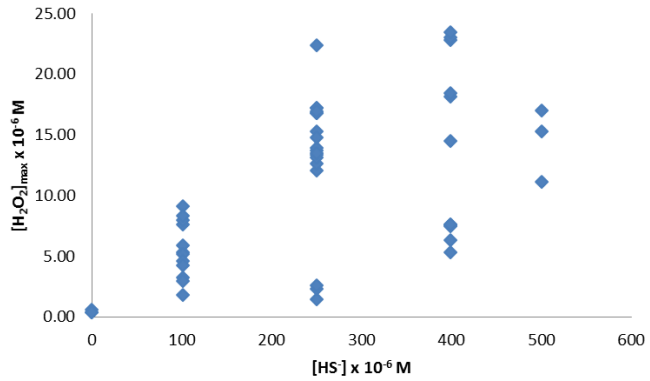

Figure 3.10. Hydrogen peroxide maximum concentration measured plotted against hydrogen sulfide concentration. All matrix runs are represented by a unique point.

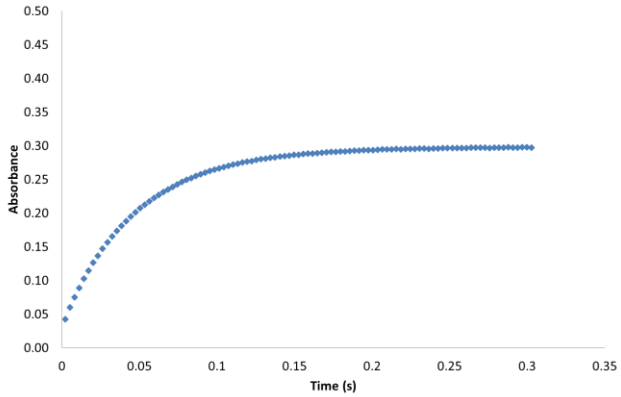

Figure 3.11: Change in absorbance at 562 nm obtained from monitoring the reaction of Fe(II) (17.5×10^{-6} M) with a stoichiometric excess of Ferrozine reagent at pH = 7 using a Hi-Tech Scientific SF-61 DX2 Double Mixing Stopped-Flow System with a Hi-Tech Scientific Control Unit and Hi-Tech Lamp Power Supply PS-678 Xenon lamp.

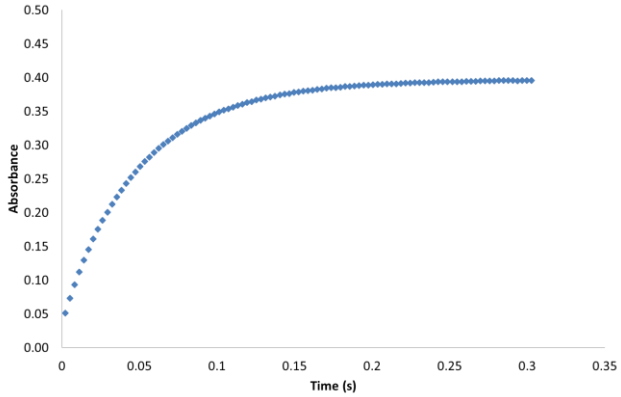

Figure 3.12: Change in absorbance at 562 nm obtained from monitoring the reaction of Fe(II) (17.5×10^{-6} M) with a stoichiometric excess of Ferrozine reagent at pH = 8 using a Hi-Tech Scientific SF-61 DX2 Double Mixing Stopped-Flow System with a Hi-Tech Scientific Control Unit and Hi-Tech Lamp Power Supply PS-678 Xenon lamp.

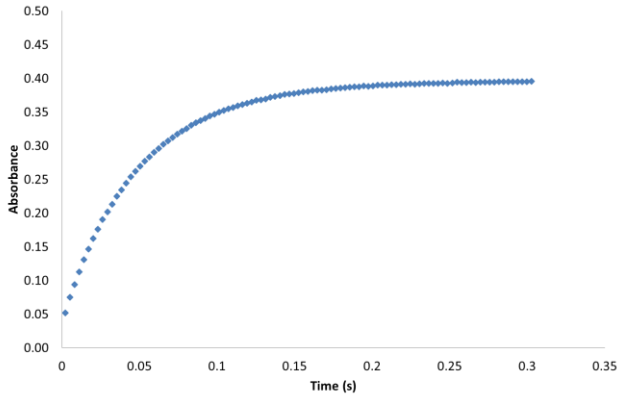

Figure 3.13: Change in absorbance at 562 nm obtained from monitoring the reaction of Fe(II) (17.5×10^{-6} M) with a stoichiometric excess of Ferrozine reagent at pH = 9 using a Hi-Tech Scientific SF-61 DX2 Double Mixing Stopped-Flow System with a Hi-Tech Scientific Control Unit and Hi-Tech Lamp Power Supply PS-678 Xenon lamp.

Figure 3.14: Baruch Institute – tidal creek sediment contained 4.7% carbon, 0.4% nitrogen, 0.26% iron, and 79% water.

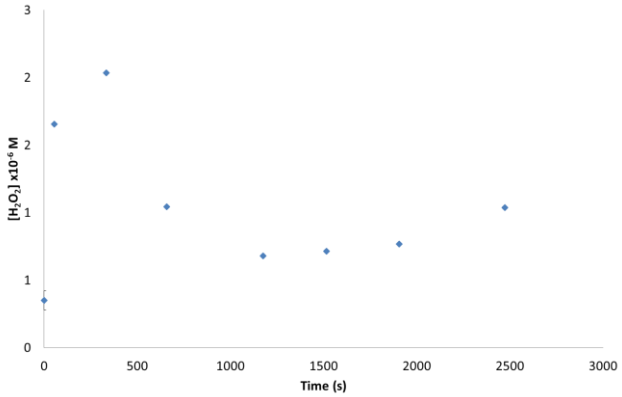

Figure 3.15: Measured hydrogen peroxide in the oxidation of 250 x10^{-6} M HS^- in the presence of 150 x10^{-6} M added Fe(III). Data reported is the average of 3 replicate measurements, with error bars corresponding to 1 standard deviation.

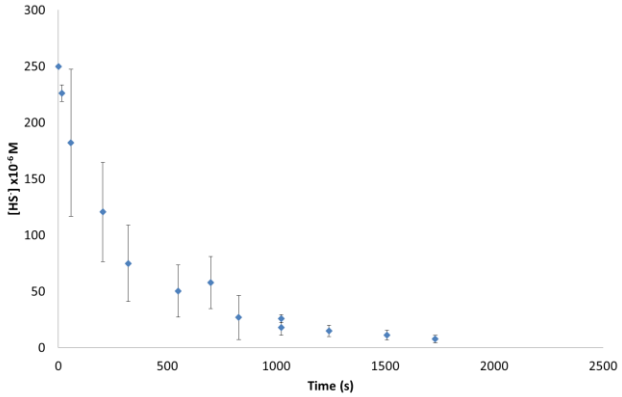

Figure 3.16: Measured sulfide in the oxidation of 250 x10^{-6} M HS^- in the presence of 150 x10^{-6} M added Fe(III). Data reported is the average of 3 replicate measurements, with error bars corresponding to 1 standard deviation.

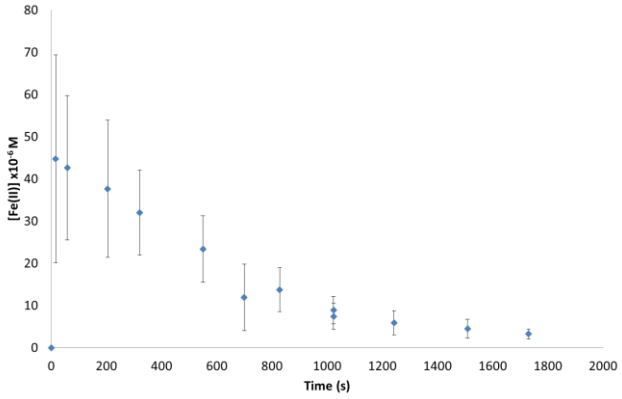

Figure 3.17: Measured Fe(II) in the oxidation of 250 x10^{-6} M HS^- in the presence of 150 x10^{-6} M added Fe(III). Data reported is the average of 3 replicate measurements, with error bars corresponding to 1 standard deviation.

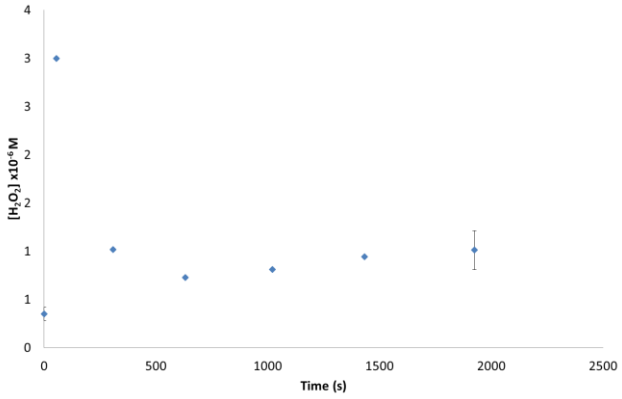

Figure 3.18: Measured hydrogen peroxide in the co-oxidation of 101 x10^{-6} M HS^- and 61 x10^{-6} M Fe(II) in the presence of 61 x10^{-6} M added Fe(III). Data reported is the average of 3 replicate measurements, with error bars corresponding to 1 standard deviation.

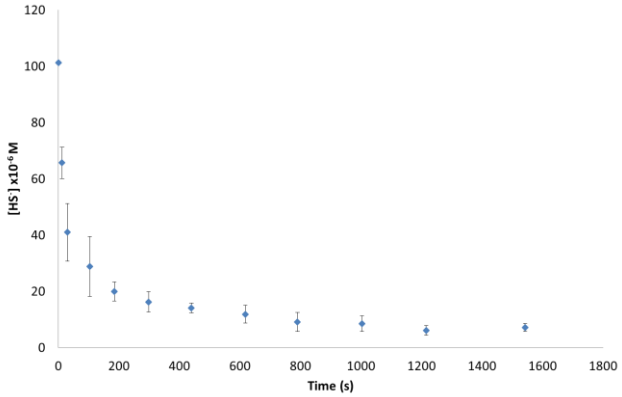

Figure 3.19: Measured sulfide in the co-oxidation of 101 x10^{-6} M HS^- and 61 x10^{-6} M Fe(II) in the presence of 61 x10^{-6} M added Fe(III). Data reported is the average of 3 replicate measurements, with error bars corresponding to 1 standard deviation.

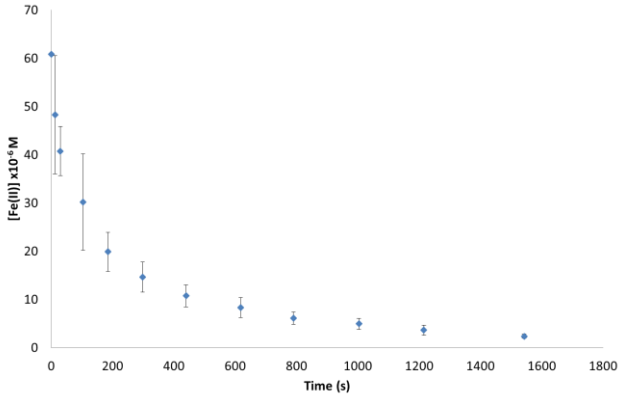

Figure 3.20: Measured Fe(II) in the co-oxidation of 101 x10^{-6} M HS^- and 61 x10^{-6} M Fe(II) in the presence of 61 x10^{-6} M added Fe(III). Data reported is the average of 3 replicate measurements, with error bars corresponding to 1 standard deviation.

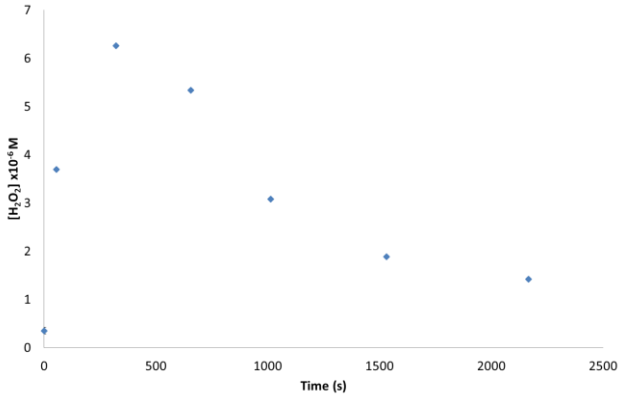

Figure 3.21: Measured hydrogen peroxide in the co-oxidation of 399 x10^{-6} M HS^- and 61 x 10^{-6} M Fe(II) in the presence of 61 x10^{-6} M added Fe(III). Data reported is the average of 3 replicate measurements, with error bars corresponding to 1 standard deviation.

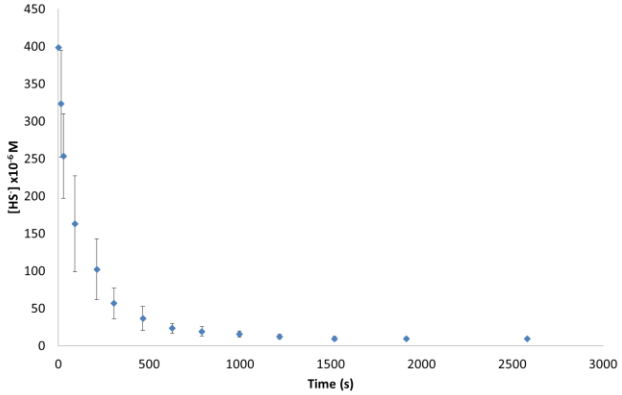

Figure 3.22: Measured sulfide in the co-oxidation of 399 x10^{-6} M HS^- and 61 x10^{-6} M Fe(II) in the presence of 61 x10^{-6} M added Fe(III). Data reported is the average of 3 replicate measurements, with error bars corresponding to 1 standard deviation.

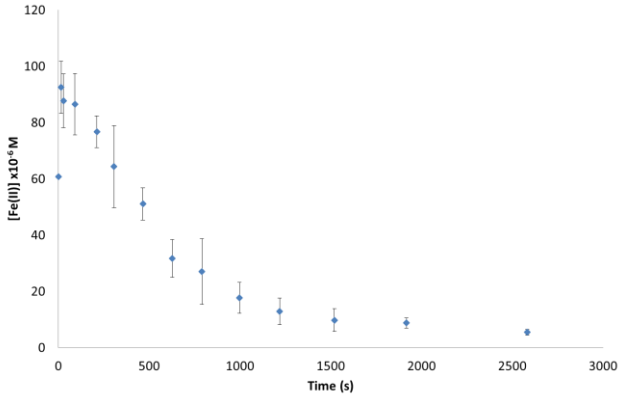

Figure 3.23: Measured Fe(II) in the co-oxidation of 399 x10^{-6} M HS^- and 61 x10^{-6} M Fe(II) in the presence of 61 x10^{-6} M added Fe(III). Data reported is the average of 3 replicate measurements, with error bars corresponding to 1 standard deviation.

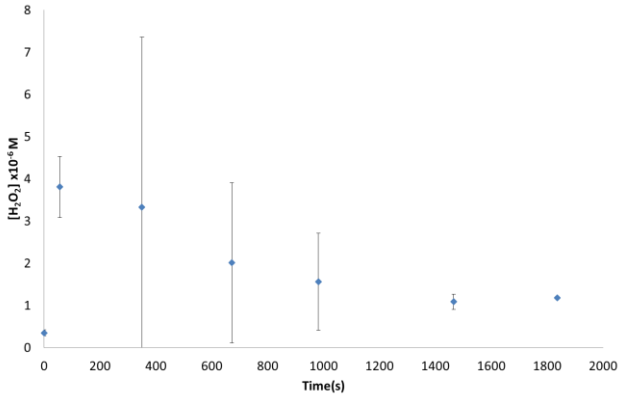

Figure 3.24: Measured hydrogen peroxide in the co-oxidation of 101 x10^{-6} M HS^- and 61 x 10^{-6} M Fe(II) in the presence of 239 x10^{-6} M added Fe(III). Data reported is the average of 3 replicate measurements, with error bars corresponding to 1 standard deviation.

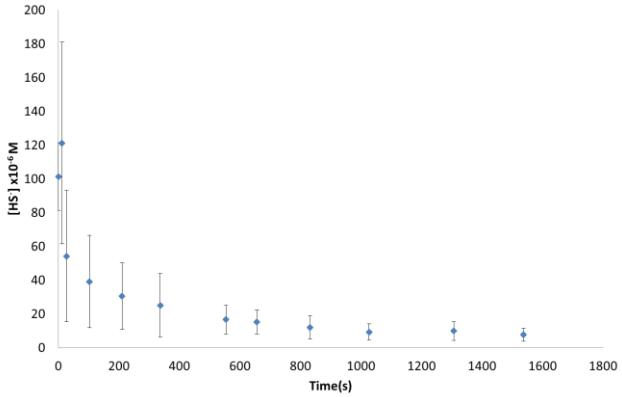

Figure 3.25: Measured sulfide in the co-oxidation of 101 x10^{-6} M HS^- and 61 x10^{-6} M Fe(II) in the presence of 239 x10^{-6} M added Fe(III). Data reported is the average of 3 replicate measurements, with error bars corresponding to 1 standard deviation.

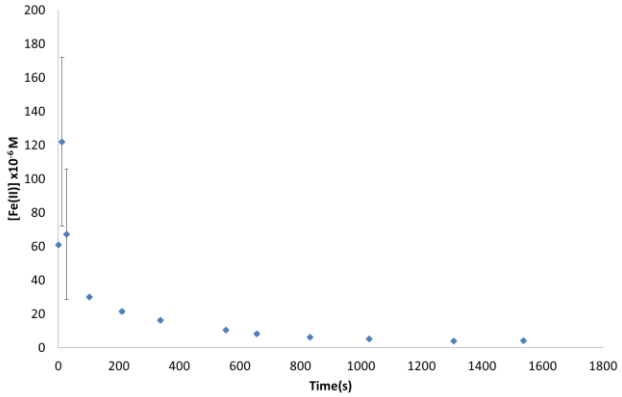

Figure 3.26: Measured Fe(II) in the co-oxidation of 101 x10^{-6} M HS^- and 61 x10^{-6} M Fe(II) in the presence of 239 x10^{-6} M added Fe(III). Data reported is the average of 3 replicate measurements, with error bars corresponding to 1 standard deviation.

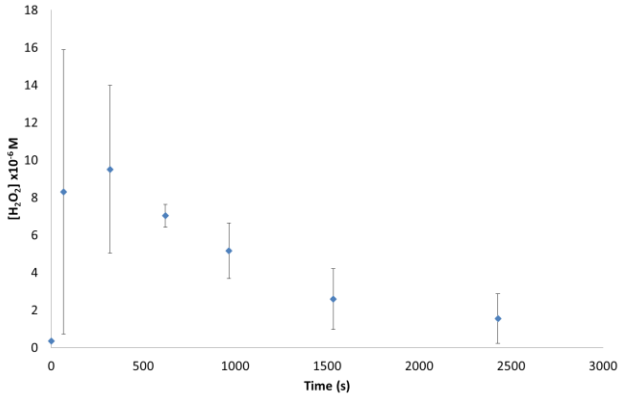

Figure 3.27: Measured hydrogen peroxide in the co-oxidation of 399 x10^{-6} M HS^- and 61 x 10^{-6} M Fe(II) in the presence of 239 x10^{-6} M added Fe(III). Data reported is the average of 3 replicate measurements, with error bars corresponding to 1 standard deviation.

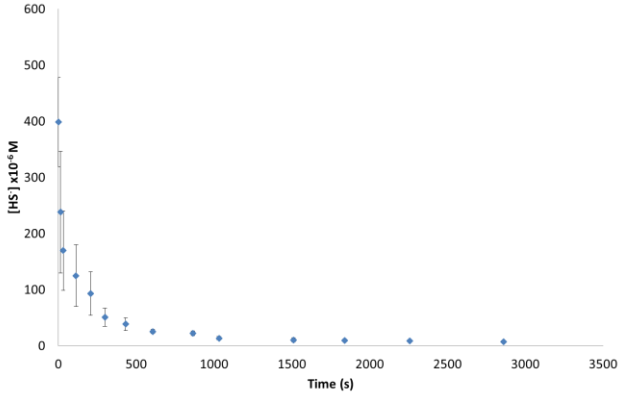

Figure 3.28: Measured sulfide in the co-oxidation of 399 x10^{-6} M HS^- and 61 x10^{-6} M Fe(II) in the presence of 239 x10^{-6} M added Fe(III). Data reported is the average of 3 replicate measurements, with error bars corresponding to 1 standard deviation.

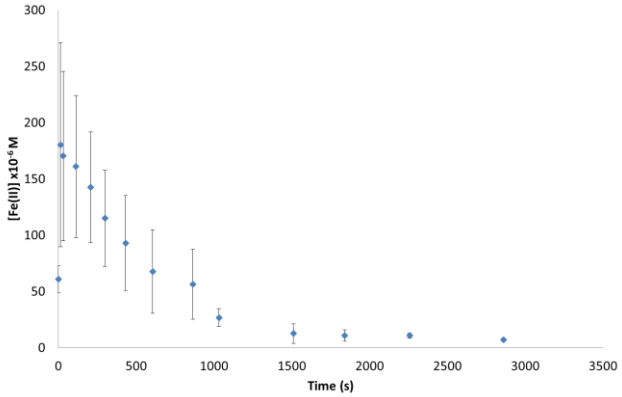

Figure 3.29: Measured Fe(II) in the co-oxidation of 399 x10^{-6} M HS^- and 61 x10^{-6} M Fe(II) in the presence of 239 x10^{-6} M added Fe(III). Data reported is the average of 3 replicate measurements, with error bars corresponding to 1 standard deviation.

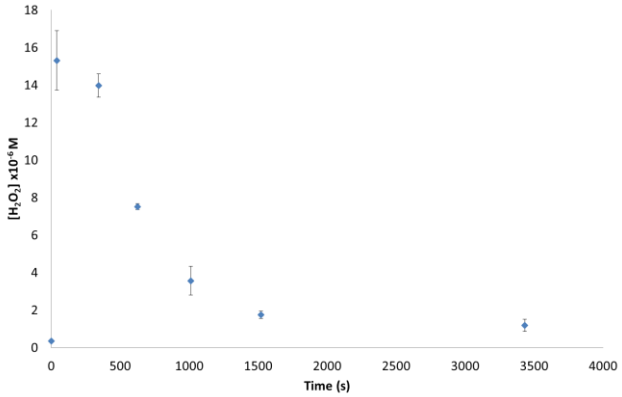

Figure 3.30: Measured hydrogen peroxide in the co-oxidation of 250 x10^{-6} M HS^- and 150 x10^{-6} M Fe(II) in the presence of no added Fe(III). Data reported is the average of 3 replicate measurements, with error bars corresponding to 1 standard deviation.

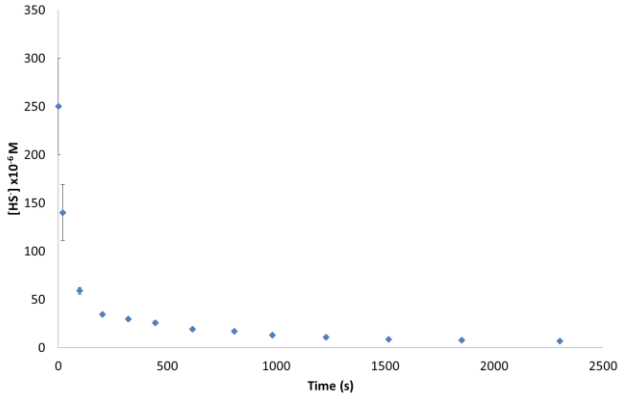

Figure 3.31: Measured sulfide in the co-oxidation of 250 x10^{-6} M HS^- and 150 x10^{-6} M Fe(II) in the presence of no added Fe(III). Data reported is the average of 3 replicate measurements, with error bars corresponding to 1 standard deviation.

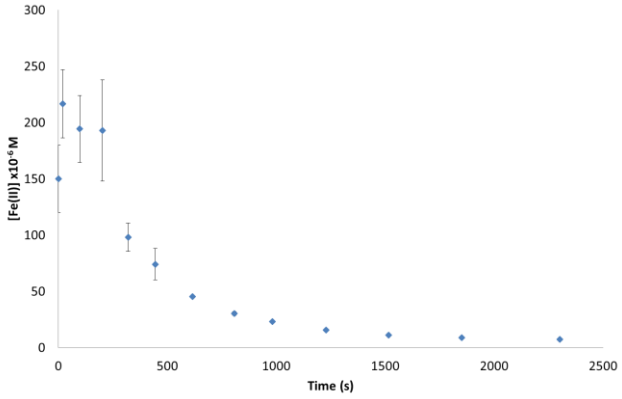

Figure 3.32: Measured Fe(II) in the co-oxidation of 250 x10^{-6} M HS^- and 150 x10^{-6} M Fe(II) in the presence of no added Fe(III). Data reported is the average of 3 replicate measurements, with error bars corresponding to 1 standard deviation.

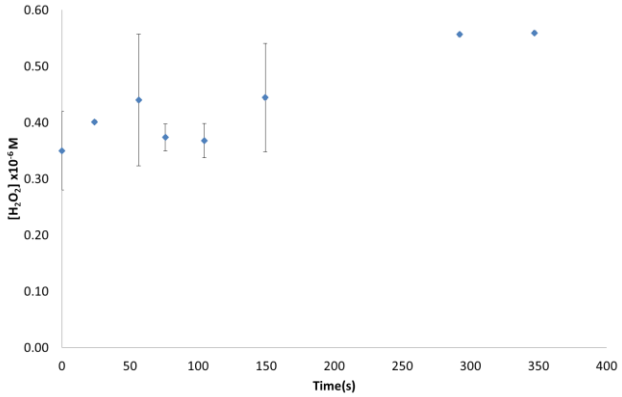

Figure 3.33: Measured hydrogen peroxide in the oxidation of 150 x10^{-6} M Fe(II) in the presence of 150 x10^{-6} M added Fe(III). Data reported is the average of 3 replicate measurements, with error bars corresponding to 1 standard deviation.

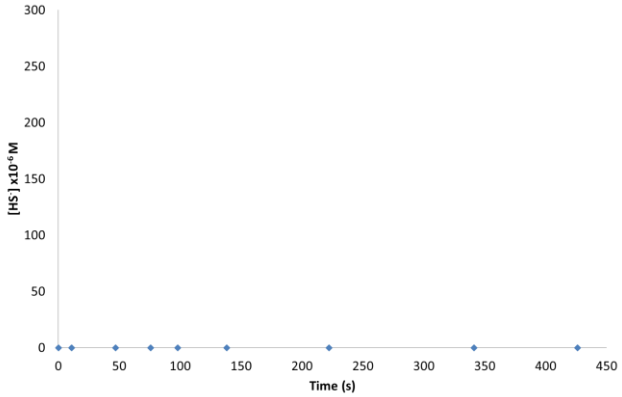

Figure 3.34: Measured sulfide in the oxidation of 150 x10^{-6} M Fe(II) in the presence of 150 x10^{-6} M added Fe(III). Data reported is the average of 3 replicate measurements, with error bars corresponding to 1 standard deviation.

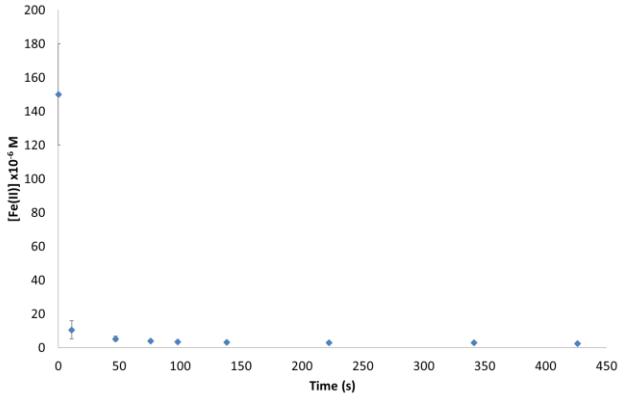

Figure 3.35: Measured Fe(II) in the oxidation of 150 $x10^{-6}$ M Fe(II) in the presence of 150 $x10^{-6}$ M added Fe(III). Data reported is the average of 3 replicate measurements, with error bars corresponding to 1 standard deviation.

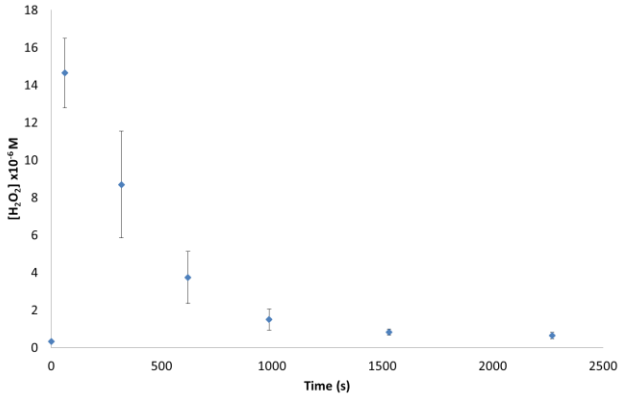

Figure 3.36: Measured hydrogen peroxide in the co-oxidation of 250 $x10^{-6}$ M HS^- and 150 $x10^{-6}$ M Fe(II) in the presence of 150 $x10^{-6}$ M added Fe(III). Data reported is the average of 6 replicate measurements, with error bars corresponding to 1 standard deviation.

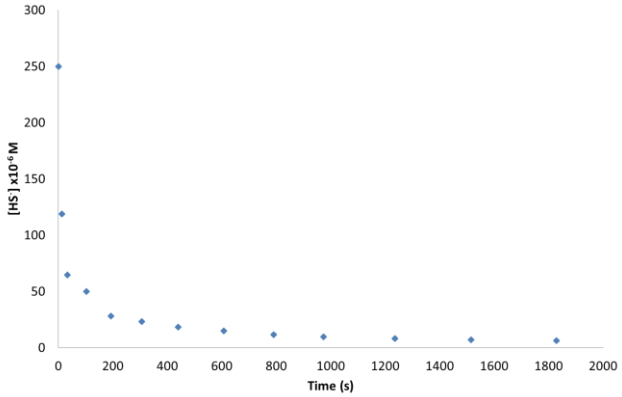

Figure 3.37: Measured sulfide in the co-oxidation of 250 x10^{-6} M HS^- and 150 x10^{-6} M Fe(II) in the presence of 150 x10^{-6} M added Fe(III). Data reported is the average of 6 replicate measurements, with error bars corresponding to 1 standard deviation.

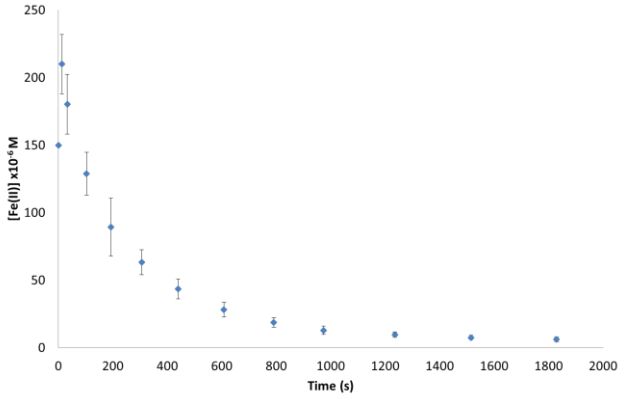

Figure 3.38: Measured Fe(II) in the co-oxidation of 250 x10^{-6} M HS^- and 150 x10^{-6} M Fe(II) in the presence of 150 x10^{-6} M added Fe(III). Data reported is the average of 6 replicate measurements, with error bars corresponding to 1 standard deviation.

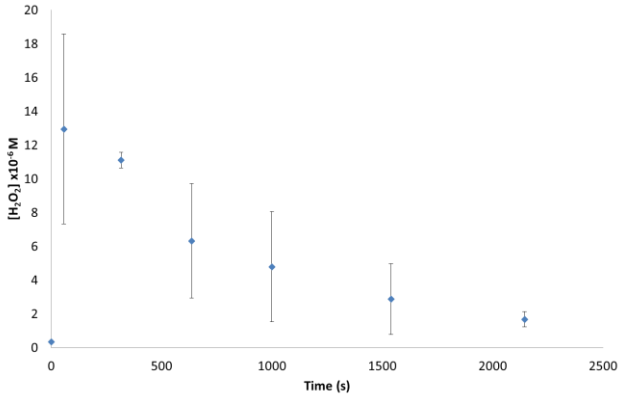

Figure 3.39: Measured hydrogen peroxide in the co-oxidation of 500 x10^{-6} M HS^- and 150 x10^{-6} M Fe(II) in the presence of 150 x10^{-6} M added Fe(III). Data reported is the average of 3 replicate measurements, with error bars corresponding to 1 standard deviation.

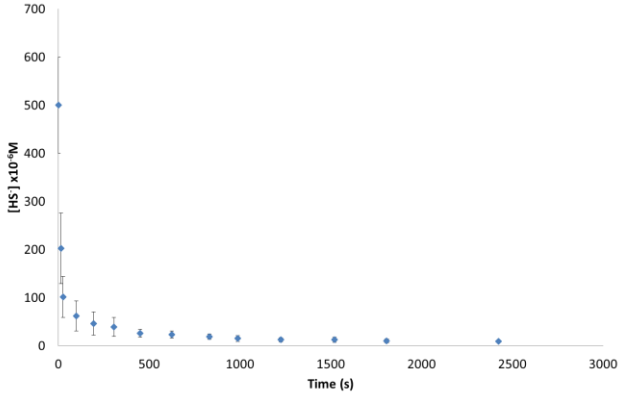

Figure 3.40: Measured sulfide in the co-oxidation of 500 x10^{-6} M HS^- and 150 x10^{-6} M Fe(II) in the presence of 150 x10^{-6} M added Fe(III). Data reported is the average of 3 replicate measurements, with error bars corresponding to 1 standard deviation.

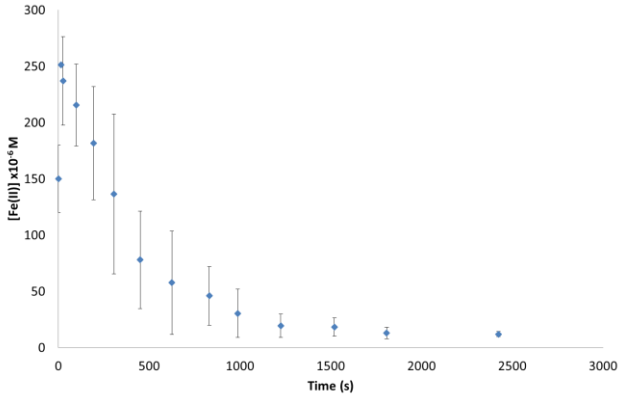

Figure 3.41: Measured Fe(II) in the co-oxidation of 500 x10^{-6} M HS^- and 150 x10^{-6} M Fe(II) in the presence of 150 x10^{-6} M added Fe(III). Data reported is the average of 3 replicate measurements, with error bars corresponding to 1 standard deviation.

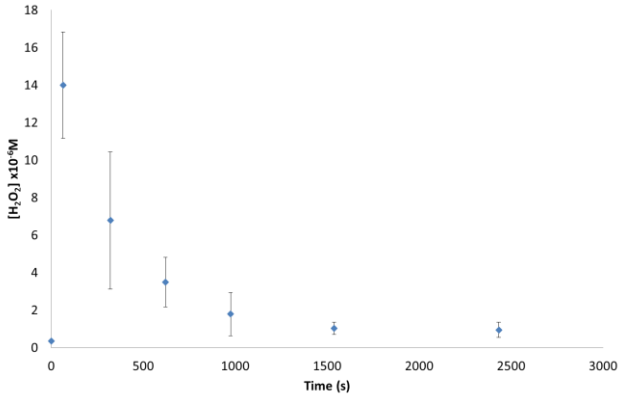

Figure 3.42: Measured hydrogen peroxide in the co-oxidation of 250 x10^{-6} M HS^- and 150 x10^{-6} M Fe(II) in the presence of 300 x10^{-6} M added Fe(III). Data reported is the average of 3 replicate measurements, with error bars corresponding to 1 standard deviation.

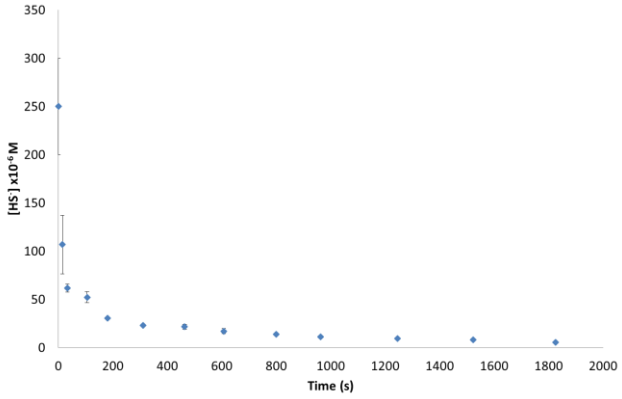

Figure 3.43: Measured sulfide in the co-oxidation of 250 x10^{-6} M HS^- and 150 x10^{-6} M Fe(II) in the presence of 300 x10^{-6} M added Fe(III). Data reported is the average of 3 replicate measurements, with error bars corresponding to 1 standard deviation.

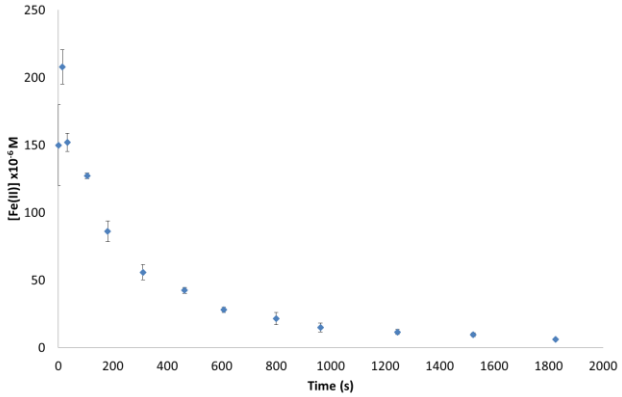

Figure 3.44: Measured Fe(II) in the co-oxidation of 250 x10^{-6} M HS^- and 150 x10^{-6} M Fe(II) in the presence of 300 x10^{-6} M added Fe(III). Data reported is the average of 3 replicate measurements, with error bars corresponding to 1 standard deviation.

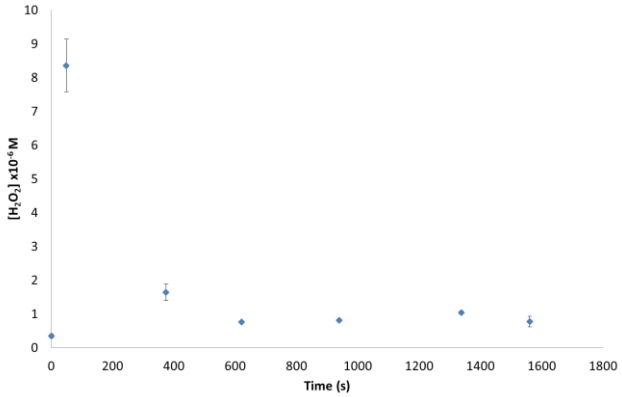

Figure 3.45: Measured hydrogen peroxide in the co-oxidation of 61 x10^{-6} M HS^- and 239 x10^{-6} M Fe(II) in the presence of 101 x10^{-6} M added Fe(III). Data reported is the average of 3 replicate measurements, with error bars corresponding to 1 standard deviation.

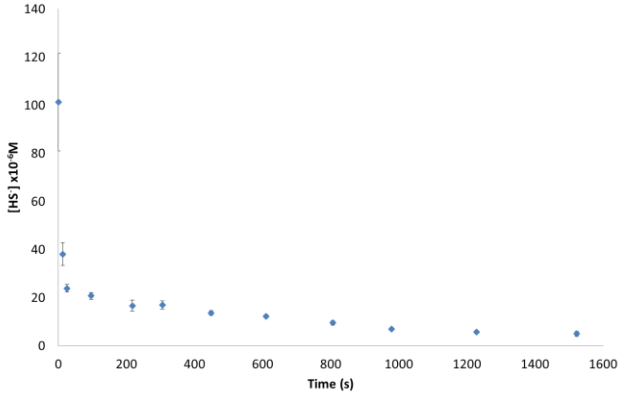

Figure 3.46: Measured sulfide in the co-oxidation of 61 x10^{-6} M HS^- and 239 x10^{-6} M Fe(II) in the presence of 101 x10^{-6} M added Fe(III). Data reported is the average of 3 replicate measurements, with error bars corresponding to 1 standard deviation.

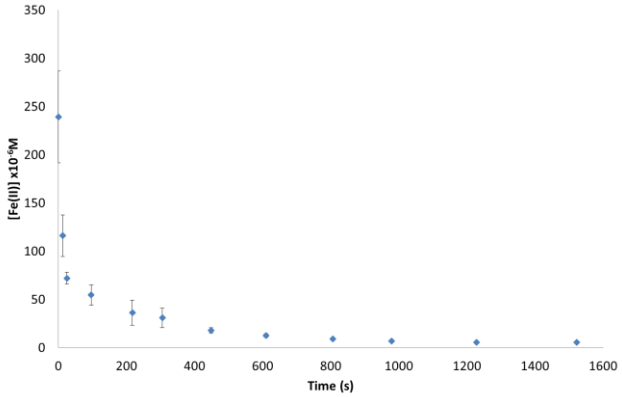

Figure 3.47: Measured Fe(II) in the co-oxidation of 61 x10^{-6} M HS^- and 239 x10^{-6} M Fe(II) in the presence of 101 x10^{-6} M added Fe(III). Data reported is the average of 3 replicate measurements, with error bars corresponding to 1 standard deviation.

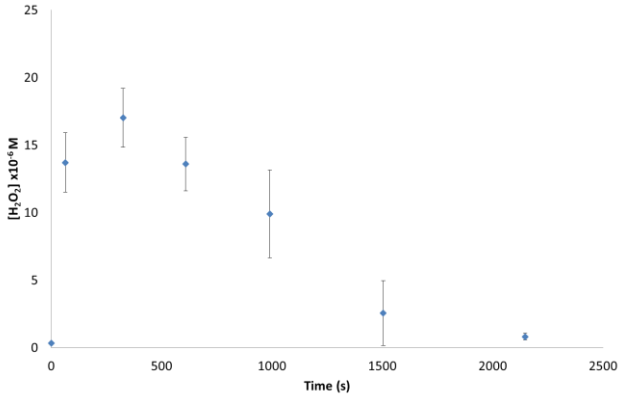

Figure 3.48: Measured hydrogen peroxide in the co-oxidation of 399 x10^{-6} M HS^- and 239 x10^{-6} M Fe(II) in the presence of 61 x10^{-6} M added Fe(III). Data reported is the average of 3 replicate measurements, with error bars corresponding to 1 standard deviation.

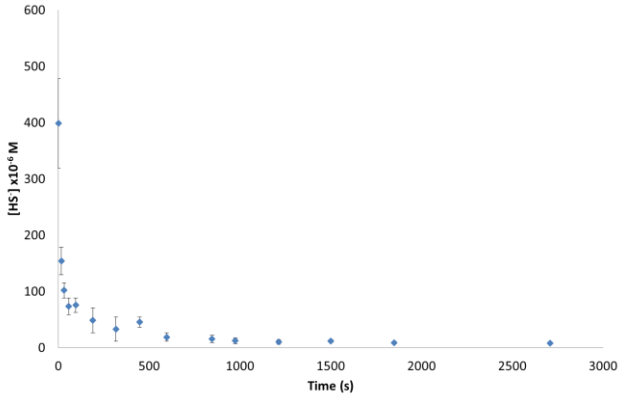

Figure 3.49: Measured sulfide in the co-oxidation of 399 x10^{-6} M HS^- and 239 x10^{-6} M Fe(II) in the presence of 61 x10^{-6} M added Fe(III). Data reported is the average of 3 replicate measurements, with error bars corresponding to 1 standard deviation.

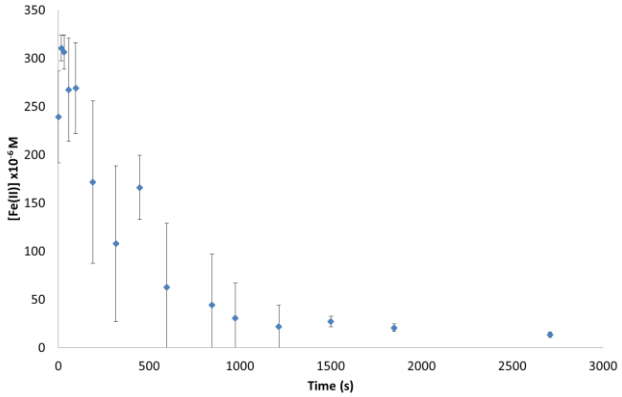

Figure 3.50: Measured Fe(II) in the co-oxidation of 399 x10^{-6} M HS^- and 239 x10^{-6} M Fe(II) in the presence of 61 x10^{-6} M added Fe(III). Data reported is the average of 3 replicate measurements, with error bars corresponding to 1 standard deviation.

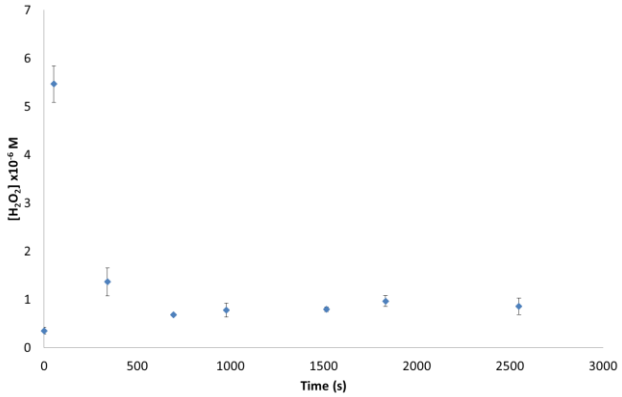

Figure 3.51: Measured hydrogen peroxide in the co-oxidation of 101 x10^{-6} M HS^- and 239 x10^{-6} M Fe(II) in the presence of 239 x10^{-6} M added Fe(III). Data reported is the average of 3 replicate measurements, with error bars corresponding to 1 standard deviation.

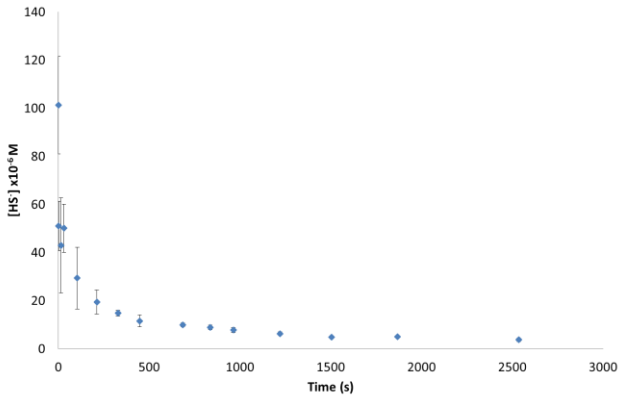

Figure 3.52: Measured sulfide in the co-oxidation of 101 x10^{-6} M HS^- and 239 x10^{-6} M Fe(II) in the presence of 239 x10^{-6} M added Fe(III). Data reported is the average of 3 replicate measurements, with error bars corresponding to 1 standard deviation.

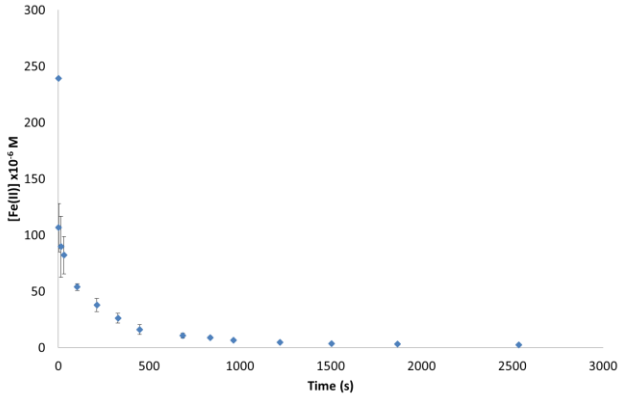

Figure 3.53: Measured Fe(II) in the co-oxidation of 101 x10^{-6} M HS^- and 239 x10^{-6} M Fe(II) in the presence of 239 x10^{-6} M added Fe(III). Data reported is the average of 3 replicate measurements, with error bars corresponding to 1 standard deviation.

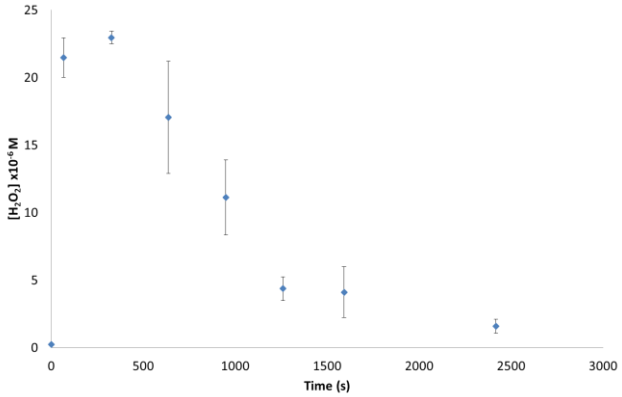

Figure 3.54: Measured hydrogen peroxide in the co-oxidation of 399 x10^{-6} M HS^- and 239 x10^{-6} M Fe(II) in the presence of 239 x10^{-6} M added Fe(III). Data reported is the average of 3 replicate measurements, with error bars corresponding to 1 standard deviation.

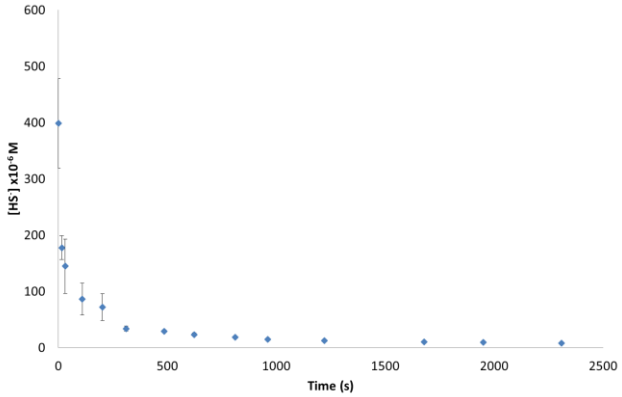

Figure 3.55: Measured sulfide in the co-oxidation of 399 x10^{-6} M HS^- and 239 x10^{-6} M Fe(II) in the presence of 239 x10^{-6} M added Fe(III). Data reported is the average of 3 replicate measurements, with error bars corresponding to 1 standard deviation.

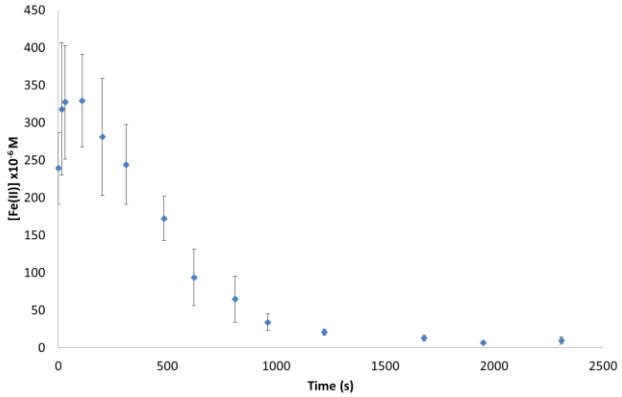

Figure 3.56: Measured Fe(II) in the co-oxidation of 399 x10^{-6} M HS^- and 239 x10^{-6} M Fe(II) in the presence of 239 x10^{-6} M added Fe(III). Data reported is the average of 3 replicate measurements, with error bars corresponding to 1 standard deviation.

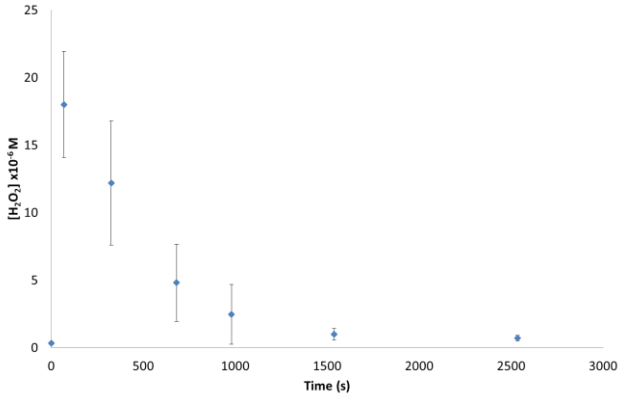

Figure 3.57: Measured hydrogen peroxide in the co-oxidation of 150 x10^{-6} M HS^- and 300 x10^{-6} M Fe(II) in the presence of 150 x10^{-6} M added Fe(III). Data reported is the average of 3 replicate measurements, with error bars corresponding to 1 standard deviation.

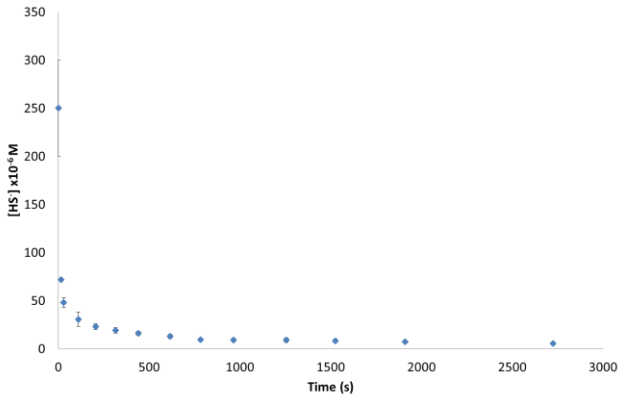

Figure 3.58: Measured sulfide in the co-oxidation of 150 x10^{-6} M HS^- and 300 x10^{-6} M Fe(II) in the presence of 150 x10^{-6} M added Fe(III). Data reported is the average of 3 replicate measurements, with error bars corresponding to 1 standard deviation.

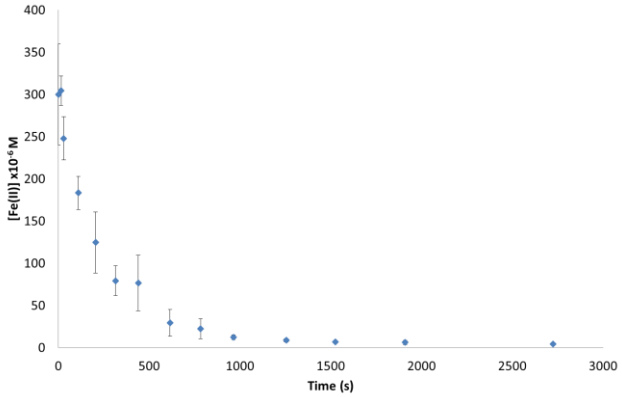

Figure 3.59: Measured Fe(II) in the co-oxidation of 150 x10^{-6} M HS^- and 300 x10^{-6} M Fe(II) in the presence of 150 x10^{-6} M added Fe(III). Data reported is the average of 3 replicate measurements, with error bars corresponding to 1 standard deviation.

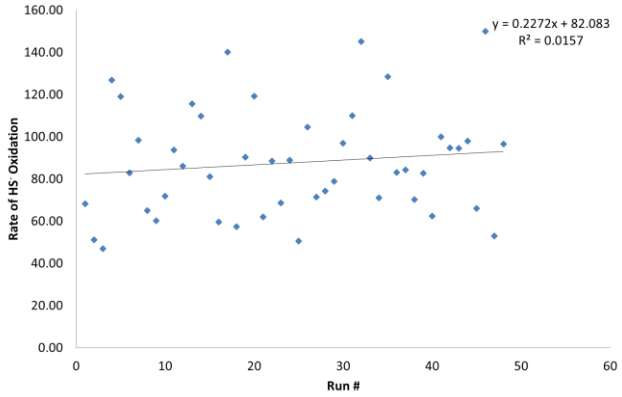

Figure 3.60: The variation of the rate of sulfide oxidation across the run order is shown to have no correlation. This indicates that there are no time dependent artifacts evident in the rate of sulfide oxidation.

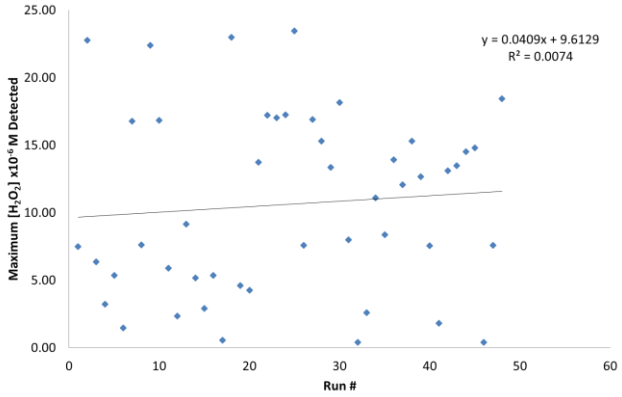

Figure 3.61: The variation of the maximum concentration of hydrogen peroxide across the run order is shown to have no correlation. This indicates that there are no time dependent artifacts evident in the maximum concentration of hydrogen peroxide detected.

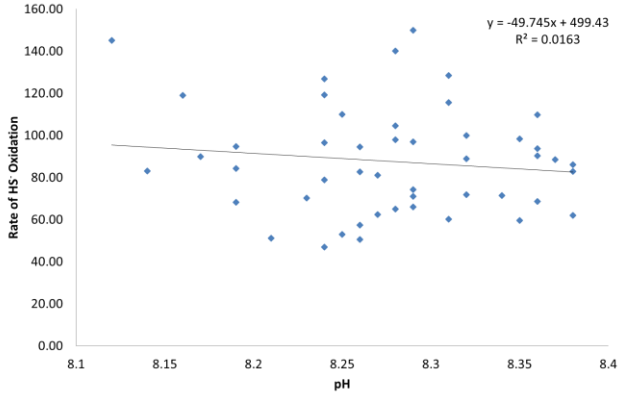

Figure 3.62: The variation of the rate of sulfide oxidation across pH is shown to have no correlation. This indicates that there are no pH dependent artifacts evident in the rate of sulfide oxidation.

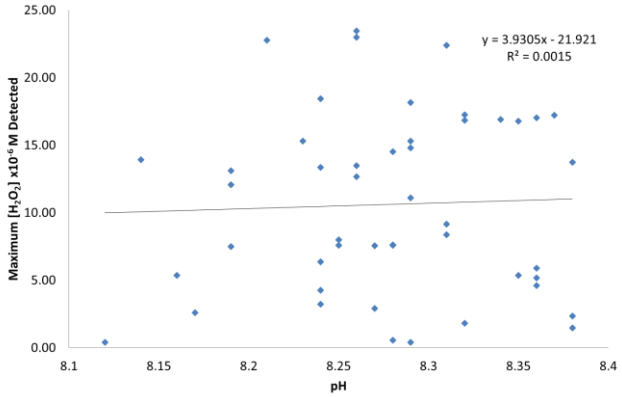

Figure 3.63: The variation of the maximum concentration of hydrogen peroxide across pH is shown to have no correlation. This indicates that there are no pH dependent artifacts evident in the maximum concentration of hydrogen peroxide detected.

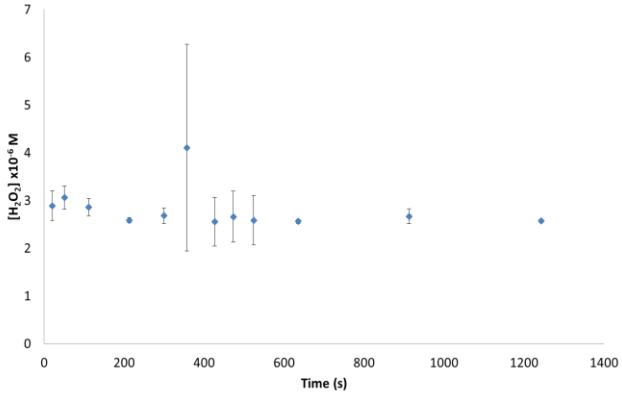

Figure 3.64: Measured hydrogen peroxide in the co-oxidation of 150 x10^{-6} M HS^- and 150 x10^{-6} M Fe(II) in the presence of 150 x10^{-6} M added Fe(III) with 30 x10^{-6} M peroxide spiked. Data reported is the average of 3 replicate measurements, with error bars corresponding to 1 standard deviation.

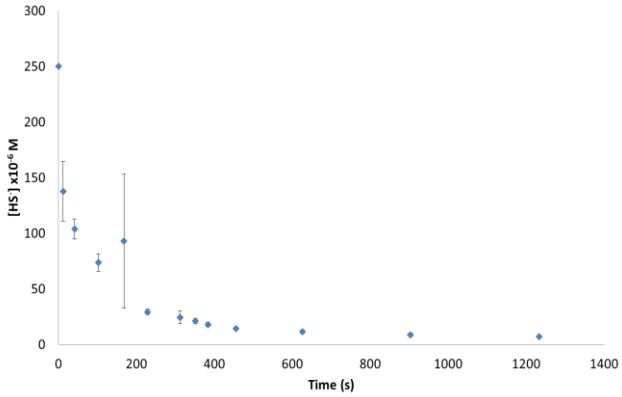

Figure 3.65: Measured sulfide in the co-oxidation of 150 x10^{-6} M HS^- and 150 x10^{-6} M Fe(II) in the presence of 150 x10^{-6} M added Fe(III) with 30 x10^{-6} M peroxide spiked. Data reported is the average of 3 replicate measurements, with error bars corresponding to 1 standard deviation.

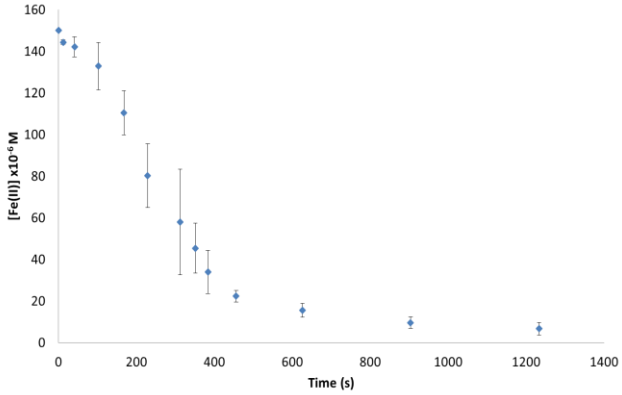

Figure 3.66: Measured Fe(II) in the co-oxidation of 150 x10^{-6} M HS^- and 150 x10^{-6} M Fe(II) in the presence of 150 x10^{-6} M added Fe(III) with 30 x10^{-6} M peroxide spiked. Data reported is the average of 3 replicate measurements, with error bars corresponding to 1 standard deviation.

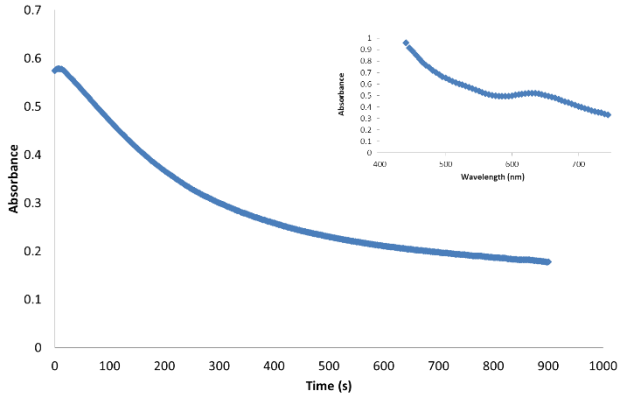

Figure 3.67: Formation and decay of amorphous FeS at 630 nm over time; Measurements begin ~2s post injection of anoxic 945 x10^{-6} M Fe(II) into a 250 x10^{-6} M sulfide solution. See insert for spectrum.

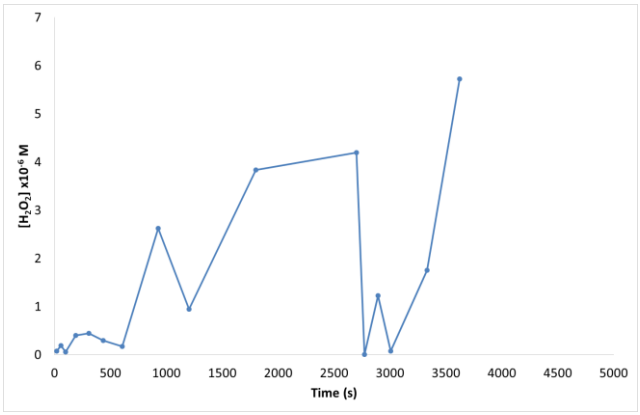

Figure 3.68: Measured hydrogen peroxide in the oxidation of 600 x10^{-6} M HS^- in a 10.0 g/L slurry of Bread and Butter Creek Sediment with 3.00 x10^{-6} M HS^- spiked at 2741 s.

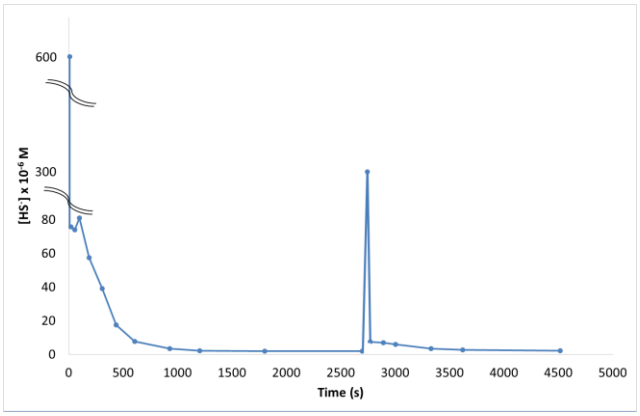

Figure 3.69: Measured sulfide in the oxidation of 600 x10^{-6} M HS^- in a 10.0 g/L slurry of Bread and Butter Creek Sediment with 3.00 x10^{-6} M HS^- spiked at 2741 s.

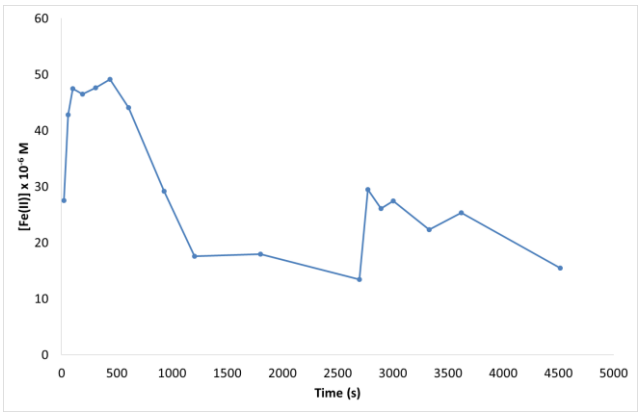

Figure 3.70: Measured Fe(II) in the oxidation of 6.00 x10^{-6} M HS^- in a 10.0 g/L slurry of Bread and Butter Creek Sediment with 3.00 x10^{-6} M HS^- spiked at 2741 s.

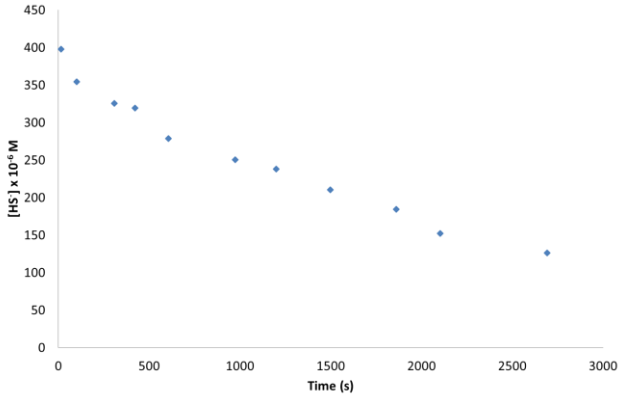

Figure 3.71: Initial [HS^-] = 398 x 10^{-6} M; slow loss over time (not catalytic oxidation as seen with added metals). Fe(II) and peroxide were below detection limit for all time points sampled. When peroxide was added to the same at t = 0, peroxide remained stable$\left(\frac{d[H_2O_2]}{dt} = 0\right)$, and there was no change in the rate of sulfide loss (volatilization or oxidation).

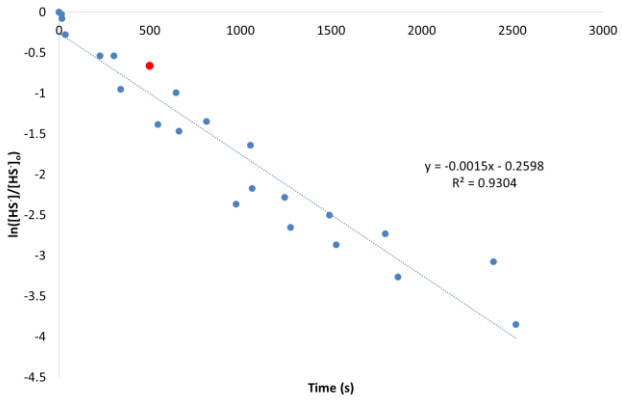

Figure 3.72: Initial [HS^-] = 250 x 10^{-6} M; [Fe(III)] = 150 x 10^{-6} M, [Fe(II)] at nominal 0. The pseudo-first order rate constant of 0.0015 s^{-1} results in a half-life (indicated by ●) of sulfide in this system of 462 s.

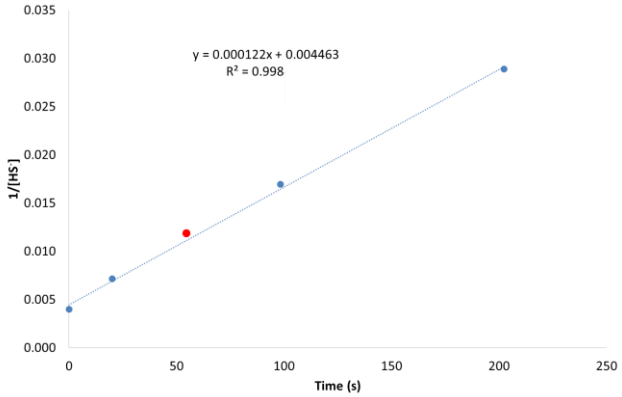

Figure 3.73: Initial [HS^-] = 250 x 10^{-6} M; [Fe(II)] = 150 x 10^{-6} M, [Fe(III)] at nominal 0. The second order rate constant of 0.000122 $M^{-1}s^{-1}$ results in a half-life (indicated by ●) of sulfide in this system of 33 s.

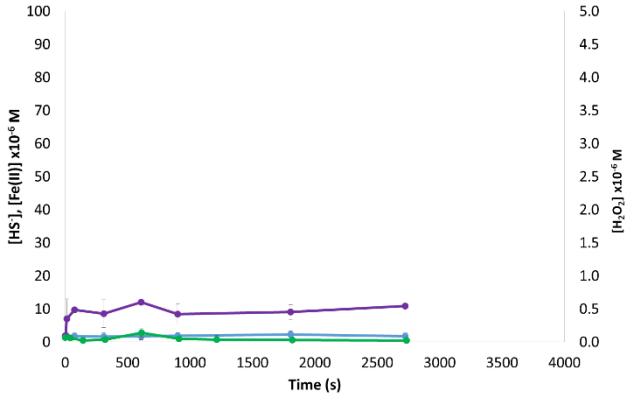

Figure 3.74: Concentration of hydrogen sulfide, $Fe(II)_{aq}$, and H_2O_2 in slurry of Bread and Butter Creek sediment (10.00 g sediment/L) with no added sulfide are shown. Error bars shown are ±1 standard deviation based on *n* = 3 experiments.

Table 3.4. Initial Reactor Conditions

Exp #	Run #	Fe(II) x 10^{-6} M	Fe(III) x 10^{-6} M	HS^- x 10^{-6} M
20	1	60.8	239	399
22	2	239	239	399
15	3	60.8	60.8	399
9	4	60.8	239	101
11	5	239	239	101
25	6	0	150	250
48	7	150	150	250
21	8	60.8	239	399
30	9	300	150	250
28	10	300	150	250
12	11	239	239	101
27	12	0	150	250
4	13	239	60.8	101
10	14	239	239	101
3	15	60.8	60.8	101
14	16	60.8	60.8	399
38	17	150	150	0
23	18	239	239	399
8	19	60.8	239	101
2	20	60.8	60.8	101
32	21	150	0	250
46	22	150	150	250
42	23	150	150	500
36	24	150	300	250
24	25	239	239	399
5	26	239	60.8	101
31	27	150	0	250
41	28	150	150	500
44	29	150	150	250
16	30	239	60.8	396
7	31	60.8	239	101
39	32	150	150	0
26	33	0	150	250
40	34	150	150	500
6	35	239	60.8	101
43	36	150	150	250
35	37	150	300	250
33	38	150	0	250
34	39	150	300	250
19	40	60.8	239	399

1	41	60.8	60.8	101
45	42	150	150	250
47	43	150	150	250
17	44	239	60.8	399
29	45	300	150	250
37	46	150	150	0
13	47	60.8	60.8	399
18	48	239	60.8	399

Table 3.5. Full Anova Report

ANOVA for Response Surface Quadratic Model

Analysis of variance table [Partial sum of squares - Type III]

Source	Sum of Squares	df	Mean Square	F Value	p-value Prob > F
Model	57.69	9	6.41	47.61	< 0.0001
[Fe(II)]	20.16	1	20.16	149.71	< 0.0001
[Fe(III)]	0.08	1	0.08	0.58	0.4523
$[HS^-]$	23.10	1	23.10	171.57	< 0.0001
[Fe(II)][Fe(III)]	0.15	1	0.15	1.13	0.2948
$[Fe(II)][HS^-]$	2.12	1	2.12	15.77	0.0003
$[Fe(III)] [HS^-]$	0.31	1	0.31	2.29	0.1382
$[Fe(II)]^2$	3.29	1	3.29	24.43	< 0.0001
$[Fe(III)]^2$	0.0001	1	0.0001	0.001	0.9745
$[HS^-]^2$	8.68	1	8.68	64.44	< 0.0001
Residual	5.12	38	0.13		
Lack of Fit	2.52	5	0.50	6.42	0.0003
Pure Error	2.59	33	0.08		
Cor Total	62.80	47			
Std. Dev.	0.37	R-Squared			0.919
Mean	3.05	Adj R-Squared			0.899
C.V. %	12.03	Pred R-Squared			0.869
PRESS	8.24	Adeq Precision			22.508

Table 3.6. Coded Confidence Interval of β_x						
	β_x		Standard	95% CI	95% CI	
Factor (x)	Estimate	df	Error	Low	High	VIF
Intercept	3.8193	1	0.1494	3.5169	4.1216	NA
[Fe(II)]	0.7014	1	0.0573	0.5853	0.8174	1.0000
[Fe(III)]	0.0435	1	0.0573	-0.0725	0.1596	1.0000
$[HS^-]$	0.7509	1	0.0573	0.6348	0.8669	1.0000
[Fe(II)][Fe(III)]	-0.0796	1	0.0749	-0.2312	0.0721	1.0000
$[Fe(II)][HS^-]$	0.2974	1	0.0749	0.1458	0.4490	1.0000
$[Fe(III)]\ [HS^-]$	0.1134	1	0.0749	-0.0382	0.2651	1.0000
$[Fe(II)]^2$	-0.3441	1	0.0696	-0.4849	-0.2032	1.3324
$[Fe(III)]^2$	0.0022	1	0.0696	-0.1387	0.1431	1.3324
$[HS^-]^2$	-0.5587	1	0.0696	-0.6996	-0.4178	1.3324

Chapter 4: Geochemical Formation of Hydrogen Peroxide in Seawater is Quenched at Lower pH[2]

Sarah A. Murphy,[1] John L. Ferry,[1,2] Timothy J. Shaw, [1,2] Shengnan Meng, [1] Benson A. Solomon.[1]*

SUMMARY PARAGRAPH

Hydrogen peroxide is a reactive oxygen species (ROS) associated with carbon cycling, the microbial generation of disinfectants and enzymatic production of halogenated organics.[91-93] Geochemical or aphotic formation of hydrogen peroxide is a consequence of the microbial utilization of alternate electron acceptors including Fe(III) and SO_4^{2-} in oxygen-poor environments, such as pore waters in shallow sediments.[3] Pore water efflux to surface waters can be driven by tidal processes or advective groundwater movement and bears the corresponding reduced forms of these electron acceptors into oxygenated overlying waters, including Fe(II) and HS^-.[94] Their subsequent Fe-catalyzed oxidation by atmospheric oxygen results in the formation of a suite of ROS, including the superoxide anion radical and hydrogen peroxide.[1, 95] However, the yield of hydrogen peroxide from this reaction is sensitive to pH and Fe speciation. Here we show that changes in marine pH associated with predicted ocean acidification are sufficient to quench hydrogen peroxide formation, potentially reducing it by an order of magnitude

[2] To be submitted.

relative to current marine conditions (e.g. from $18.3x10^{-6}$ M to $2.01x10^{-6}$ M over the range of conditions studied). The unexpected effect of changing pH is shown to be a consequence of the interaction of hydrogen peroxide with an intermediate oxidation state of HS^-, sulfite. Peroxide yield and the interfering reaction are reported across five coastal conditions based on sediments samples drawn from across the littoral zone, including the low tide line, surf line, barrier dunes, a dredged ship channel and forested salt marsh edge. Although all sediments measured produced some hydrogen peroxide the highest yields and greatest pH sensitivity was observed for organic rich marsh sediments where Fe speciation was dominated by ferrihydrite.

INTRODUCTION

ROS are produced in surface waters through a manifold of photochemical, microbial and geochemical processes.[96] Photoproduction of ROS is limited by light intensity and the availability of reactive initiators such as Fe containing complexes, nitrate and dissolved organic matter.[97-98] The rate of photochemical ROS production is difficult to estimate on the global scale, but anthropogenic activities are contributing to conditions that favor increases in ROS; specifically referencing increased insolation associated with ozone depletion and ice cover loss and localized increases in photosensitizers, e.g. increased nitrate loading from fertilizer use.[99-100] The ultimate ecological impact of enhanced ROS input is difficult to forecast but photoderived ROS have been demonstrated to be genotoxic to both single-celled and multicellular marine organisms.[101-103] Geochemical ROS production is linked to mass transport of solutions containing reduced metals across the sediment/water interface and its global scale is correspondingly more difficult to estimate. However these processes are also potentially

subject to global scale anthropogenic disruption, particularly associated with changes in surface water pH driven by increases in anthropogenic carbon dioxide (e.g. ocean acidification).[104-105] Recent work coupling ocean acidification models with the natural geographical distribution of seawater pH indicates a natural variation of ±0.5 units against an atmospherically driven reduction of potentially 0.2 units is likely within the next two hundred years.[106] Accommodating pH fluctuations across this scale is an important step for estimating potential impact on geochemical ROS formation.

Estuaries and river deltas are geographic integrators for waterborne natural and anthropogenic carbon during its transport from continental sources to the oceans. As such, ROS generated in these environments have the potential to exert a broad geographical impact despite their brief lifetimes. They are also subject to tidally driven fluctuations in groundwater flow, pH, salinity, dissolved metals and total carbon.[107-109] This study reports the effect of changing pH on the yield of hydrogen peroxide in these critical environments. A series of sediment samples were drawn across the marine littoral zone in South Carolina, US, proceeding from the surf line inland to the landward edge of a *Spartina* dominated salt marsh.

Samples were sieved, dried and analyzed for metal content. Acid digestion of sediments showed that crystalline Fe oxides were the dominant source of transition metals except at the forested swamp edge, where Fe speciation was more amorphous determined by ascorbate leeching analysis[110]. These samples were then resuspended in pH-adjusted seawater to model the effects of tidally driven porewater export into oxic overlying waters.[1, 3] The pH was adjusted from 8.5 to 7.0 to bracket the natural pH variability in the near shore environment and the projected change in ocean pH due to

increasing atmospheric carbon dioxide over the next 200 years. After equilibration of the sediment sample in aqueous solution, sulfide was spiked in and aliquots of known volume were periodically withdrawn for analysis of sulfide accessible Fe, HS^- and H_2O_2 for concentration over time.[61, 111-112] Sufficient hydrogen sulfide was added to the suspensions to mimic concentrations of hydrogen sulfide commonly found in marshes and at the sediment-water interface where sulfide rich oxygen depleted groundwater mixes with marine water.

Hydrogen peroxide generation was immediate upon addition of hydrogen sulfide under all conditions (Figure 4.1 and inset). From a maximum instantaneous yield of 18.3 x 10^{-6} M at pH = 8.25 to a minimum of 2.01 x10^{-6} M at pH = 7, there is nearly a 10 fold decrease in maximum hydrogen peroxide measured. Solution pH was varied according to projections based on anthropogenic carbon dioxide emissions. The sediment sample from the forested marsh edge, which had the highest amorphous iron oxide content, was the most vulnerable to changes in pH and showed the greatest change.

The complex nature of the samples limits the ability to pursue an exclusive mechanism to explain this decline in yield. However, one possible explanation is the reaction between hydrogen peroxide and a partial oxidation product of hydrogen sulfide, the sulfite ion[101]

$$HSO_3^- + H_2O_2 \rightleftarrows HSO_4^- + H_2O \qquad \text{Eqn. 4.1}$$

Qualitative analysis of sulfur oxidation products was achieved through direct injection of 0.2 micron-filtered samples from the suspensions into a quadrupole-time of

flight mass spectrometer (see methods section). This analysis indicated the co-presence of sulfide, sulfite, thiosulfate and sulfate during the oxidation. The bimolecular rate constant for the reduction of hydrogen peroxide by sulfite ions is strongly dependent on pH, varying from $2*10^{-5}$ at pH 8.2 to $2*10^{-2}$ at pH 6.8, increasing linearly with ionic strength. This is particularly true for sulfite at pH below 7.9, where a significant percentage of total sulfite is expressed as bisulfite. This observation suggests the hypothesis that hydrogen sulfite quenches apparent hydrogen peroxide formation through scavenging hydrogen peroxide (and possibly other ROS). This hypothesis was tested by measuring hydrogen peroxide degradation rates in bisulfite solution as a function of pH. Measured degradation rates from these experiments inversely correlated with peroxide yields vs pH (Figure 4.2 and inset).

The effects of this process on organic matter (carbon) were qualitatively interrogated by indicated by high resolution orbitrap mass spectrometry, which showed an approximate ~ 15% increase in the number of peaks in the 100-500 m/z range. Nominally this outcome suggested sulfide-driven ROS formation may have a direct impact on organic carbon speciation in coastal sediments. If these transformations are borne out in field measurements, one implication is that ocean acidification may impact coastal microbial degradation of organics by inhibiting the formation of low molecular weight, water soluble carbon sources.

AUTHOR ADDRESS

1. Department of Chemistry and Biochemistry, University of South Carolina, Columbia SC 29208. 2. Nanocenter at the University of South Carolina, Columbia SC 29208.

KEYWORDS nanomaterial, climate change, hydroxyl radical, mineralization

Table 4.1. Metal Content of Sediment Samples.

Metal	Marsh	Canal	Dune	Beach Face	Surf Line	Control
Fe_{total} (ppm)	38876	3830	1653	63085	3382	353
$Fe_{amorphous}$ (ppm)	9838	387	59	61	286	-
Cu (ppm)	27	47	4.0	4.7	2.7	24
Co (ppm)	8.5	10	0.4	0.8	0.9	0.2
Ni (ppm)	25	4.7	1.7	2.2	2.9	2.0
Mn (ppm)	257	126	65	5773	49	12

Sediment samples were obtained from the top 2 cm. The Control sediment was sand, triple washed with aqua regia followed by a triple rinse with 18 MΩ deionized water to purify the sample of solution accessible metals.

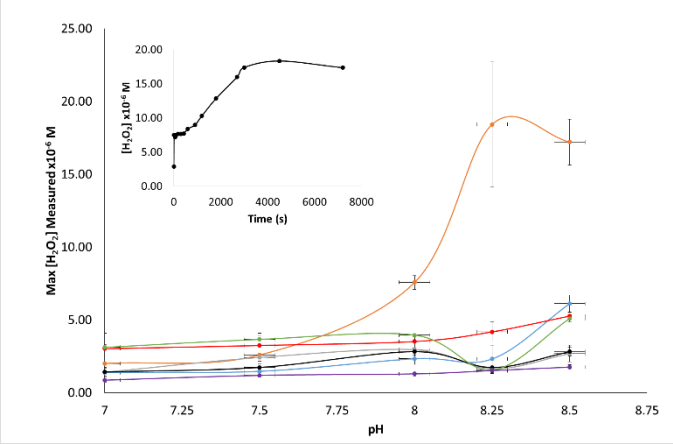

Figure 4.1. Maximum concentration of hydrogen peroxide measured as a function of pH. ● – Seep, ● – Marsh, ● – Dune, ● – Canal, ● – Swash zone, ● – Acid washed sand, ● – No sediment added. Error bars correspond to 1 standard deviation, *n=3*. Inset – typical hydrogen peroxide profile over time.

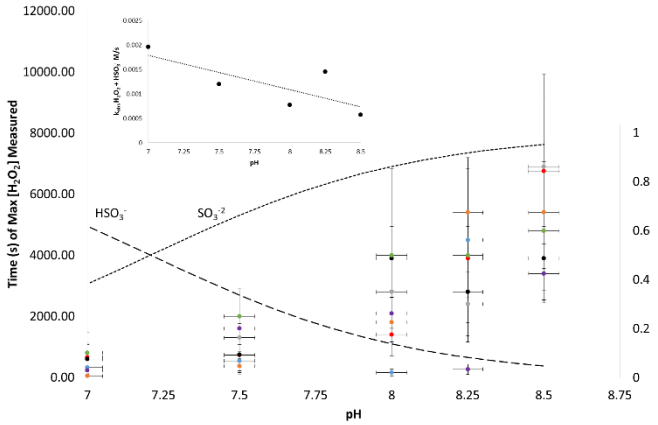

Figure 4.2. Time required to achieve the hydrogen peroxide maximum as a function of pH. ● – Seep, ● – Marsh, ● – Dune, ● – Canal, ● – Swash zone, ● – Acid washed sand, ● – No sediment added. Error bars correspond to 1 standard deviation, *n=3*. Lines indicate sulfite speciation: dotted – sulfite, dashed – bisulfite. Inset – Observed rate of hydrogen peroxide and bisulfite across Ph

Chapter 5: Conclusions

The cooxidation of Fe(II) and HS^- results in the formation of ROS, including hydrogen peroxide. The introduction of additional HS^- sustains ROS production, indicating the catalytic role of Fe in the system. Although several species of Fe may co-exist in environmental samples, assays for different forms in sediment samples indicated that only colloidal material was efficient at the HS^- to ROS conversion of reductive equivalents. The role of organic C in the system is as yet unquantified but circumstantial evidence exists for it as a sink of ROS and potential source of superoxide.

In chapter 2, biogeochemical sources of ROS were discussed and global contributions were calculated. Focusing on sulfide as a primary electron donor for oxygen reduction, positive and negative contributions of the sulfur cycle to ROS and the potential impact on carbon mineralization was discussed. Net production and consumption rates of ROS were discussed as a function of pH, with changes in global ROS budgets calculated.

Chapter 3 discussed a geochemical ROS production mechanism, namely sulfide as an electron donor to oxygen reduction through a catalyst, iron. Multivariate experimental modeling resulted in a numerical model which was tested against environmental sediment sample suspensions. Despite the large excess of organic carbon in the suspensions, the *in vitro* model predicted the outcome of ROS generated when sulfide was spiked into the suspension to within at least the 90% confidence interval. Speculatively, it was suggested that the constant negative bias was a result of H_2O_2 production during the peroxidation of organic carbon post oxidation by hydroxyl radical.

The high concentration of natural organic materials in the studied system indicated they were certainly the primary sink for secondary ROS such as HO• generated during the process. It was suggested that the impact of sulfide as an electron donor will be significant to micropollutant fate and global carbon cycling. Additionally, sulfide was proposed as an abiotic link between microbial metabolism and carbon oxidation.

Given known and predicted changes in ocean pH, it was critical to extend the results of chapter 3 to lower pH values. Chapter 4 discusses the changes in ROS production from sulfide and Fe across a range of pH values bracketing predicted ocean pH changes over the next 200 years. Data showed a significant decrease in ROS concentration at lower pH values, indicating potentially an order of magnitude decrease in sulfide generated ROS micropollutant degradation and carbon mineralization.

References

1. Murphy, S. A.; Solomon, B. M.; Meng, S.; Copeland, J. M.; Shaw, T. J.; Ferry, J. F. Geochemical production of reactive oxygen species from biogeochemically reduced Fe *Environ. Sci. Technol.* **2014**
2. Diaz, J. M. et al Widespread Production of Extracellular Superoxide by Heterotrophic Bacteria, *Science* **2013**
3. Luther, G. W. The Role of One- and Two-Electron Transfer Reactions in Forming Thermodynamically Unstable Intermediates as Barries in Multi-Electron Redox Reactions. *Aquat. Geochem.* 16(3). **2010.** 395-420.
4. Yucel, M. et al Hydrothermal vents as a kinetically stable source of iron-sulphide-bearing nanoparticles to the ocean, *Nat. Geosci.* **2011**
5. Rothschild, W. G.; Allen, A. O. Studies in the radiolysis of ferrous sulfate solutions. III. Air-free solutions at higher pH. Radiat. Res. 8, 101-110, 1958.].
6. Stumm, W.; Lee, G. F., Oxygenation of ferrous iron. *Ind. Eng. Chem.* **1961,** *53*, (2), 143-146.
7. Staehelin, J.; Hoigne, J., Decomposition of ozone in water - rate of initiation by hydroxide ions and hydrogen-peroxide. *Environ. Sci. Technol.* **1982,** *16*, (10), 676-681.
8. Gonzalez-Davila, M.; Santana-Casiano, J. M.; Millero, F. J., Oxidation of iron(II) nanomolar with H_2O_2 in seawater. *Geochim. Cosmochim. Ac.* **2005,** *69*, (1), 83-93.
9. Betts, R. H. and Voss, R. H. Can. J. Chem, **48,** 2035 (1970)
10. Buxton, G. V.; Greenstock, C. L.; Helman, W. P.; Ross, A. B. Critical review of rate constants for reactions of hydrated electrons, hydrogen atoms and hydroxyl radicals (OH/O-) in aqueous solution. *J. Phys. Chem. Ref. Data*. 1988, 17. 513-886.
11. Johnston, S. L. and Voordouw, G. Sulfate-Reducing Bacteria Lower Sulfur-Mediated Pitting Corrosion under Conditions of Oxygen Ingress *Environ. Sci. Technol.* 46, **2012**;
12. Luther, G.W. *et al* Seasonal iron cycling in the salt-marsh sedimentary encironment: the importance of ligand complexes with iron(II) and iron(III) in the dissolution of iron(III) minerals and pyrite, respectively, *Environ. Sci. Technol.*, 40(1-2) **1992.** 81-103.
13. Hoffman, M. R. and Edwards, J. O. Kinetics of the Oxidation of Sulfite by Hydrogen Peroixde in Acidic Solution. *J. Phys. Chem.* 79 (20) **1975**.
14. Bowles, M. W. *et al*. Global rates of marine sulfate reduction and implications for sub-sea-floor metabolic activities. Science 344. 889-891. **2014**.
15. Hansard, S. P., Vermilyea, A. W., Voelker, B. M. Measurements of superoxide radical concentration and decay kinetics in the Gulf of Alaska, *Deep Sea Res. I.* **2010**.

16. Vermilyea, A. W.; Hansard, S. P.; Voelker, B. M. Dark production of hydrogen peroxide in the Gulf of Alaska. *Limnol. Oceanogr.*, 55(2), **2010**, 580-588
17. Taillefert, M.; Neuhuber, S.; Bristow, G. The effect of tidal forcing on biogeochemical processes in intertidal salt marsh sediments. *Geochem. Trans.* **2007** doi: 10.1186/1467-4866-8-6
18. Mills, G.; Schmidt, K. H.; Matheson, M. S.; Meisel, D. Thermal and photochemical reactions of sulfhydryl radicals. Implications for colloid photocorrosion. *J. Phys. Chem.* **1987**, 91, 1590-1596.;
19. Veltwisch, D., E. Janata, and K.D. Asmus, Primary Processes in the Reaction of Oh-Radicals with Sulfoxides. *Journal of the Chemical Society-Perkin Transactions 2,* **1980**(1): p. 146-153;
20. Asada, K.; Kanematsu, S. Reactivity of thiols with superoxide radicals. *Agr. Biol. Chem.* **1976**, 40, 1891-1892.
21. Yao, W.S. and F.J. Millero, Oxidation of hydrogen sulfide by hydrous Fe(III) oxides in seawater. *Mar. Chem.*, **1996**. 52(1). 1-16.
22. Huie, R.E. and C.L. Clifton, Temperature-Dependence of the Rate Constants for Reactions of the Sulfate Radical, SO_4^-, with Anions. *J. Phys.Chem.*, **1990**. 94(23): p. 8561-8567.
23. Huie, R.E., C.L. Clifton, and P. Neta, Electron-Transfer Reaction-Rates and Equilibria of the Carbonate and Sulfate Radical-Anions. *Radiat. Phys. Chem.*, **1991**. 38(5): p. 477-481. 50.
24. Huie, R.E. and Neta, P. Rate Constants for Some Oxidations of S(IV) by Radicals in Aqueous- Solutions. *Atmos. Environ.*, **1987**. 21(8): p. 1743-1747.
25. Jiang, P.Y., *et al*., Pulse-Radiolysis Study of Concentrated Sulfuric-Acid-Solutions - Formation Mechanism, Yield and Reactivity of Sulfate Radicals. *Journal of the Chemical Society-Faraday Transactions*. **1992**. 88(12): 1653-1658.
26. Karmann, W., G. Meissner, and A. Henglein, Pulsradiolyse Des Schwefelwasserstoffs in Wassriger Losung. *Zeitschrift Fur Naturforschung Part B-Chemie Biochemie Biophysik Biologie Und Verwandten Gebiete*, **1967**. B 22(3)
27. Kumar, M., Rao, M. H., and Moorthy, P. N. Transient Species Involved in Radiation Polymerization of Aqueous Divinyl Sulfone - a Pulse-Radiolysis Study. *Radiat. Phys. Chem.*, **1990**. 36(6): 811-814.
28. Nevin, K. P.; Lovley, D. R., Potential for nonenzymatic reduction of Fe(III) via electron shuttling in subsurface sediments. *Environ. Sci. Technol.* **2000,** *34*, (12), 2472-2478.
29. Fan, S. M., Photochemical and biochemical controls on reactive oxygen and iron speciation in the pelagic surface ocean. *Mar. Chem.* **2008,** *109*, (1-2), 152-164.
30. Faust, B. C., Photochemistry of clouds, fogs, and aerosols. *Environ. Sci. Technol.* **1994,** *28*, (5), A217-A222.
31. Haag, W. R.; Hoigne, J., Photo-sensitized oxidation in natural water via $^{\cdot}OH$ radical. *Chemosph.* **1985,** *14*, (11/12), 1659-1671.
32. Petasne, R. G.; Zika, R. G., Fate of superoxide in coastal sea water. *Nature* **1987,** *325*, (6104), 516-518.

33. Wardman, P.; Candeias, L. P., Fenton chemistry: An introduction. *Radiat. Res.* **1996,** *145*, (5), 523-531.
34. Voelker, B. M.; Morel, F. M. M.; Sulzberger, B., Iron redox cycling in surface waters: Effects of humic substances and light. *Environ. Sci. Technol.* **1997,** *31*, (4), 1004-1011.
35. Barb, W. G.; Baxendale, J. H.; George, P.; Hargrave, K. R., Reactions of ferrous and ferric ions with hydrogen peroxide. 2. The ferric ion reaction. *T. Faraday Soc.* **1951,** *47*, (6), 591-616.
36. Barb, W. G.; Baxendale, J. H.; George, P.; Hargrave, K. R., Reactions of ferrous and ferric ions with hydrogen peroxide. 1. The ferrous ion reaction. *T. Faraday Soc.* **1951,** *47*, (5), 462-500.
37. Carey, E.; Burns, J.; DiChristina, T. J.; Taillefert, M., Formation of soluble organic-Fe(III) complexes during microbial iron reduction. *Geochim.Cosmochim. Ac.* **2005,** *69*, (10), A225-A225.
38. Carey, E.; Taillefert, M., The role of soluble Fe(III) in the cycling of iron and sulfur in coastal marine sediments. *Limnol. Oceanogr.* **2005,** *50*, (4), 1129-1141.
39. USGS Nutrients National Synthesis Project. http://water.usgs.gov/nawqa/nutrients/datasets/cycle91/
40. Luther, G. W.; Glazer, B. T.; Ma, S. F.; Trouwborst, R. E.; Moore, T. S.; Metzger, E.; Kraiya, C.; Waite, T. J.; Druschel, G.; Sundby, B.; Taillefert, M.; Nuzzio, D. B.; Shank, T. M.; Lewis, B. L.; Brendel, P. J., Use of voltammetric solid-state (micro)electrodes for studying biogeochemical processes: Laboratory measurements to real time measurements with an in situ electrochemical analyzer (ISEA). *Mar. Chem.* **2008,** *108*, (3-4), 221-235.
41. Mullaugh, K. M.; Luther, G. W.; Ma, S.; Moore, T. S.; Yucel, M.; Becker, E. L.; Podowski, E. L.; Fisher, C. R.; Trouwborst, R. E.; Pierson, B. K., Voltammetric (micro)electrodes for the in situ study of Fe^{2+} oxidation kinetics in hot springs and $S_2O_3^{2-}$ production at hydrothermal vents. *Electroanal.* **2008,** *20*, (3), 280-290.
42. Roy, M.; Martin, J. B.; Cable, J. E.; Smith, C. G., Variations of iron flux and organic carbon remineralization in a subterranean estuary caused by inter-annual variations in recharge. *Geochim. Cosmochim. Ac.* **2013,** *103*, 301-315.
43. Morgan, B.; Burton, E. D.; Rate, A. W., Iron monosulfide enrichment and the presence of organosulfur in eutrophic estuarine sediments. *Chem. Geol.* **2012,** *296*, 119-130.
44. Frommichen, R.; Kellner, S.; Friese, K., Sediment conditioning with organic and/or inorganic carbon sources as a first step in alkalinity generation of acid mine pit lake water (pH 2-3). *Environ. Sci. Technol.* **2003,** *37*, (7), 1414-1421.
45. Sholkovitz, E. R.; Shaw, T. J.; Schneider, D. L., The Geochemistry of Rare-Earth Elements in the Seasonally Anoxic Water Column and Porewaters of Chesapeake Bay. *Geochim. Cosmochim. Ac.* **1992,** *56*, (9), 3389-3402.
46. Moore, W. S.; Shaw, T. J., Chemical signals from submarine fluid advection onto the continental shelf. *J. Geophys. Res-Oceans* **1998,** *103*, (C10), 21543-21552.
47. Windom, H. L.; Moore, W. S.; Niencheski, L. F. H.; Jahrike, R. A., Submarine groundwater discharge: A large, previously unrecognized source of dissolved iron to the South Atlantic Ocean. *Mar. Chem.* **2006,** *102*, (3-4), 252-266.

48. Moore, W. S., A reevaluation of submarine groundwater discharge along the southeastern coast of North America. *Global Biogeochem. Cy.* **2010,** *24*. DOI: 10.1029/2009GB003747.
49. Moore, W. S., The Effect of Submarine Groundwater Discharge on the Ocean. *Annu. Rev. Mar. Sci.* **2010,** *2*, 59-88.
50. Porubsky, W. P.; Joye, S. B.; Moore, W. S.; Tuncay, K.; Meile, C., Field measurements and modeling of groundwater flow and biogeochemistry at Moses Hammock, a backbarrier island on the Georgia coast. *Biogeochem.* **2011,** *104*, (1-3), 69-90.
51. Krest, J. M.; Moore, W. S.; Gardner, L. R.; Morris, J. T., Marsh nutrient export supplied by groundwater discharge: Evidence from radium measurements. *Global Biogeochem. Cy.* **2000,** *14*, (1), 167-176.
52. Duncan, T.; Shaw, T. J., The mobility of rare earth elements and redox sensitive elements in the groundwater/seawater mixing zone of a shallow coastal aquifer. *Aquat. Geochem.* **2003,** *9*, (3), 233-255.
53. Cooper, W. J.; Jones, A. C.; Whitehead, R. F.; Zika, R. G., Sunlight-induced photochemical decay of oxidants in natural waters: Implications in ballast water treatment. *Environ. Sci. Technol.* **2007,** *41*, (10), 3728-3733.
54. Cooper, W. J.; Zika, R. G.; Petasne, R. G.; Plane, J. M. C., Photochemical formation of H_2O_2 in natural-waters exposed to sunlight. *Environ. Sci. Technol.* **1988,** *22*, (10), 1156-1160.
55. Zepp, R. G.; Hoigne, J.; Bader, H., Nitrate-induced photooxidation of trace organic-chemicals in water. *Environ. Sci. Technol.* **1987,** *21*, (5), 443-450.
56. Zepp, R. G.; Faust, B. C.; Hoigne, J., Hydroxyl radical formation in aqueous reaction (pH 3-8) of iron (II) with hydrogen peroxide: the photo-Fenton reaction. *Environ. Sci. Technol.* **1992,** *26*, 313-319.
57. Cline, J. D., Spectrophotometric determination of hydrogen sulfide in natural waters. *Limnol. Oceanogr.* **1969,** *14*, (3), 454-458.
58. Stookey, L. L., Ferrozine - a new spectrophotometric reagent for iron. *Anal. Chem.* **1970,** *42*, (7), 779-781.
59. Burns, J. M.; Craig, P. S.; Shaw, T. J.; Ferry, J. L., Combinatorial parameter space as an empirical tool for predicting water chemistry: Fe(II) oxidation across a watershed. *Environ. Sci. Technol.* **2011,** *45*, (9), 4023-4029.
60. Burns, J. M.; Craig, P. S.; Shaw, T. J.; Ferry, J. L., Short-Term Fe Cycling during Fe(II) Oxidation: Exploring Joint Oxidation and Precipitation with a Combinatorial System. *Environ. Sci. Technol.* **2011,** *45*, (7), 2663-2669.
61. Cooper, W. J.; Moegling, J. K.; Kieber, R. J.; Kiddle, J. J., A chemiluminescence method for the analysis of H_2O_2 in natural waters. *Mar. Chem.* **2000,** *70*, (1-3), 191-200.
62. King, D. W.; Cooper, W. J.; Rusak, S. A.; Peake, B. M.; Kiddle, J. J.; O'Sullivan, D. W.; Melamed, M. L.; Morgan, C. R.; Theberge, S. M., Flow injection analysis of H_2O_2 in natural waters using acridinium ester chemiluminescence: Method development and optimization using a kinetic model. *Anal. Chem.* **2007,** *79*, (11), 4169-4176.

63. Aller, J. Y.; Aller, R. C.; Kemp, P. F.; Chistoserdov, A. Y.; Madrid, V. M., Fluidized muds: a novel setting for the generation of biosphere diversity through geologic time. *Geobiol.* **2010,** *8*, (3), 169-178.
64. Ciglenecki, I.; Bura-Nakic, E.; Margus, M., Zinc sulfide surface formation on Hg electrode during cyclic voltammetric scan: an implication for previous and future research studies on metal sulfide systems. *J. Solid State Electr.* **2012,** *16*, (6), 2041-2046.
65. Teuchies, J.; De Jonge, M.; Meire, P.; Blust, R.; Bervoets, L., Can acid volatile sulfides (AVS) influence metal concentrations in the macrophyte Myriophyllum aquaticum? *Environ. Sci. Tech.* **2012,** *46*, (16), 9129-9137.
66. Luther, G. W.; Glazer, B.; Ma, S. F.; Trouwborst, R.; Shultz, B. R.; Druschel, G.; Kraiya, C., Iron and sulfur chemistry in a stratified lake: Evidence for iron-rich sulfide complexes. *Aquat. Geochem.* **2003,** *9*, (2), 87-110.
67. Burns, J. M.; Craig, P. S.; Shaw, T. J.; Ferry, J. L., Multivariate examination of Fe(II)/Fe(III) cycling and consequent hydroxyl radical generation. *Environ. Sci. Technol.* **2010,** *44*, (19), 7226-7231.
68. Wilson, A. M.; Morris, J. T., The influence of tidal forcing on groundwater flow and nutrient exchange in a salt marsh-dominated estuary. *Biogeochem.* **2012,** *108*, (1-3), 27-38.
69. Tobias, C. R.; Harvey, J. W.; Anderson, I. C., Quantifying groundwater discharge through fringing wetlands to estuaries: Seasonal variability, methods comparison, and implications for wetland-estuary exchange. *Limnol. Oceanogr.* **2001,** *46*, (3), 604-615.
70. Fennessey, C. M.; Jones, M. E.; Taillefert, M.; DiChristina, T. J., Siderophores are not involved in Fe(III) solubilization during anaerobic Fe(III) respiration by Shewanella oneidensis MR-1. *Appl. Environ. Microb.* **2010,** *76*, (8), 2425-2432.
71. Luther, G. W.; Glazer, B. T.; Hohmann, L.; Popp, J. I.; Taillefert, M.; Rozan, T. F.; Brendel, P. J.; Theberge, S. M.; Nuzzio, D. B., Sulfur speciation monitored in situ with solid state gold amalgam voltammetric microelectrodes: polysulfides as a special case in sediments, microbial mats and hydrothermal vent waters. *J. Environ. Monit.* **2001,** *3*, (1), 61-66.
72. Tercier-Waeber, M. L.; Taillefert, M., Remote in situ voltammetric techniques to characterize the biogeochemical cycling of trace metals in aquatic systems. *J. Environ. Monit.* **2008,** *10*, (1), 30-54.
73. Survey, United States Department of the Interior, USGS National Water Quality Assessment Data Warehouse. **2007**.
74. Brodie, B. B.; Axelrod, J.; Shore, P. A.; Udenfriend, S., Ascorbic acid in aromatic hydroxylation. 2. Products formed by reaction of substrates with ascorbic acid, ferrous ion, and oxygen. *J. Biol. Chem.* **1954,** *208*, (2), 741-750.
75. Udenfriend, S.; Clark, C. T.; Axelrod, J.; Brodie, B. B., Ascorbic acid in aromatic hydroxylation. 1. A model system for aromatic hydroxylation. *J. Biol. Chem.* **1954,** *208*, (2), 731-739.
76. Kang, S. H.; Choi, W., Oxidative degradation of organic compounds using zero-valent iron in the presence of natural organic matter serving as an electron shuttle. *Environ. Sci. Technol.* **2009,** *43*, (3), 878-883.

77. Sedlak, D. L.; Hoigne, J., Oxidation of S(IV) in atmospheric water by photooxidants and iron in the presence of copper. *Environ. Sci. Technol.* **1994,** *28*, (11), 1898-1906.
78. Sedlak, D. L.; Hoigne, J., The role of copper and oxalate in the redox cycling of iron in atmospheric waters. *Atmos. Environ. a-Gen.* **1993,** *27*, (14), 2173-2185.
79. Lutz, R. A.; Shank, T. M.; Luther, G. W.; Vetriani, C.; Tolstoy, M.; Nuzzio, D. B.; Moore, T. S.; Waldhauser, F.; Crespo-Medina, M.; Chatziefthimiou, A. D.; Annis, E. R.; Reed, A. J., Interrelationships between vent fluid chemistry, temperature, seismic activity, and biological community structure at a mussel-dominated, deep-sea hydrothermal vent along the East Pacific Rise. *J. Shellfish Res.* **2008,** *27*, (1), 177-190.
80. Ma, S.; Luther, G. W.; Keller, J.; Madison, A. S.; Metzger, E.; Emerson, D.; Megonigal, J. P., Solid-state Au/Hg microelectrode for the investigation of Fe and Mn cycling in a freshwater wetland: Implications for methane production. *Electroanal.* **2008,** *20*, (3), 233-239.
81. Ma, S. F.; Noble, A.; Butcher, D.; Trouwborst, R. E.; Luther, G. W., Removal of H_2S via an iron catalytic cycle and iron sulfide precipitation in the water column of dead end tributaries. *Estuar. Coast Shelf S* **2006,** *70*, (3), 461-472.
82. Moore, T. S.; Nuzzio, D. B.; Deering, T. W.; Taillefert, M.; Luther, G. W., Use of voltammetry to monitor O_2 using Au/Hg electrodes and to control physical sensors on an unattended observatory in the Delaware bay. *Electroanal.* **2007,** *19*, (19-20), 2110-2116.
83. Babauta, J. T.; Nguyen, H. D.; Istanbullu, O.; Beyenal, H., Microscale gradients of oxygen, hydrogen peroxide, and pH in freshwater cathodic biofilms. *Chemsuschem.* **2013,** *6*, (7), 1252-1261.
84. Hsieh, P.; Pedersen, J. Z.; Albertano, P., Generation of reactive oxygen species upon red light exposure of cyanobacteria from Roman hypogea. *Int. Biodeter. Biodegr.* **2013,** *84*, 258-265.
85. Koley, D.; Ramsey, M. M.; Bard, A. J.; Whiteley, M., Discovery of a biofilm electrocline using real-time 3D metabolite analysis. *P. Natl. Acad. Sci. USA* **2011,** *108*, (50), 19996-20001.
86. Liu, X. H.; Ramsey, M. M.; Chen, X. L.; Koley, D.; Whiteley, M.; Bard, A. J., Real-time mapping of a hydrogen peroxide concentration profile across a polymicrobial bacterial biofilm using scanning electrochemical microscopy. *P. Natl. Acad. Sci. USA* **2011,** *108*, (7), 2668-2673.
87. Bielski, B. H. J., Reevaluation of spectral and kinetic-properties of HO_2 and $O_2^{-\cdot}$ free radicals. *Photochem. Photobiol.* **1978,** *28*, (4-5), 645-649.
88. Rush, J. D.; Bielski, B. H. J., Pulse radiolytic studies of the reactions of HO_2/O_2^- with Fe(II)/Fe(III) ions - the reactivity of HO_2/O_2^- with ferric ions and its implication on the occurrence of the Haber-Weiss reaction. *J. Phys. Chem.* **1985,** *89*, (23), 5062-5066.
89. Roesler, A. J.; Gammons, C. H.; Druschel, G. K.; Oduro, H.; Poulson, S. R., Geochemistry of flooded underground mine workings influenced by bacterial sulfate reduction. *Aquat. Geochem.* **2007,** *13*, (3), 211-235.

90. Roy, M.; Martin, J. B.; Smith, C. G.; Cable, J. E., Reactive-transport modeling of iron diagenesis and associated organic carbon remineralization in a Florida (USA) subterranean estuary. *Earth Planet Sc. Lett.* **2011,** *304*, (1-2), 191-201.
91. Timko, S. A., Romera-Castillo, C., Jaffe, R. & Cooper, W. J. Photo-reactivity of natural dissolved organic matter from fresh to marine waters in the Florida Everglades, USA. *Environ. Sci.-Process Impacts.* **2014.** 16, 866-878, doi:10.1039/c3em00591g.
92. Butler, A. S., M. Mechanistic consideration of halogenating enzymes. *Nature* **2009.** 460, 848-854.
93. Abele, D., Grosspietsch, H. & Portner, H. O. Temporal fluctuations and spatial gradients of environmental P-O_2, temperature, H_2O_2 and H_2S in its intertidal habitat trigger enzymatic antioxidant protection in the capitellid worm *Heteromastus filiformis*. *Mar. Ecol. Prog. Ser.* **1998.** 163, 179-191, doi:10.3354/meps163179.
94. Porubsky, W. P., Joye, S. B., Moore, W. S., Tuncay, K. & Meile, C. Field measurements and modeling of groundwater flow and biogeochemistry at Moses Hammock, a backbarrier island on the Georgia coast. *Biogeochemistry* **2011.** 104, 69-90, doi:DOI 10.1007/s10533-010-9484-8.
95. Rickard, D. *et al.* FeS-Induced Radical Formation and Its Effect on Plasmid DNA. *Aquat Geochem* **2011.** 17, 545-566, doi:DOI 10.1007/s10498-010-9116-x.
96. Marshall, J. A., de Salas, M., Oda, T. & Hallegraeff, G. Superoxide production by marine microalgae. *Mar. Biol.* **2005.** 147, 533-540, doi:10.1007/s00227-005-1596-7.
97. Gonsior, M. *et al.* Photochemically induced changes in dissolved organic matter identified by ultrahigh resolution fourier transform ion cyclotron resonance mass spectrometry. *Environ. Sci. Technol.* **2009.** 43, 698-703 (2009).
98. Kaiser, E. & Sulzberger, B. Phototransformation of riverine dissolved organic matter (DOM) in the presence of abundant iron: Effect on DOM bioavailability. *Limnol. Ocean.* **2004.** 49, 540-554.
99. Zepp, R. G., Callaghan, T. V. & Erickson, D. J. Effects of enhanced solar ultraviolet radiation on biogeochemical cycles. *Journal of Photochemistry and Photobiology B-Biology.* **1998.** 46, 69-82, doi:10.1016/s1011-1344(98)00186-9.
100. Vitousek, P. M. *et al.* Human alteration of the global nitrogen cycle: Sources and consequences. *Ecol. Appl.* **1997.** 7, 737-750, doi:10.2307/2269431.
101. Karsten, U. *et al.* Physiological responses of polar benthic algae to ultraviolet radiation. *Bot. Mar.* **2009.** 52, 639-654, doi:10.1515/bot.2009.077.
102. Shiu, C. T. & Lee, T. M. Ultraviolet-B-induced oxidative stress and responses of the ascorbate-glutathione cycle in a marine macroalga Ulva fasciata. *J. Exp. Bot.* **2005.** 56, 2851-2865, doi:10.1093/jxb/eri277.
103. Lister, K. N., Lamare, M. D. & Burritt, D. J. Sea ice protects the embryos of the Antarctic sea urchin Sterechinus neumayeri from oxidative damage due to naturally enhanced levels of UV-B radiation. *J. Exper. Biol.* **1967-1975.** 213. doi:10.1242/jeb.039990 (2010).
104. Orr, J. C. *et al.* Anthropogenic ocean acidification over the twenty-first century and its impact on calcifying organisms. *Nature* **2005.** 437, 681-686, doi:10.1038/nature04095.

105. Hoegh-Guldberg, O. *et al.* Coral reefs under rapid climate change and ocean acidification. *Science* **2007.** 318, 1737-1742, doi:10.1126/science.1152509.
106. Hofmann, G. E. *et al.* High-Frequency Dynamics of Ocean pH: A Multi-Ecosystem Comparison. *Plos One* **2011.** 6, doi:10.1371/journal.pone.0028983.
107. Burnett, W. C., Bokuniewicz, H., Huettel, M., Moore, W. S. & Taniguchi, M. Groundwater and pore water inputs to the coastal zone. *Biogeochem.* **2003.** 66, 3-33, doi:10.1023/b:biog.0000006066.21240.53.
108. Scavia, D. *et al.* Climate change impacts on US coastal and marine ecosystems. *Estuaries* **2002.** 25, 149-164, doi:10.1007/bf02691304.
109. Bianchi, T. S. The role of terrestrially derived organic carbon in the coastal ocean: A changing paradigm and the priming effect. *P Natl Acad Sci USA* **2011.** 108, 19473-19481, doi:DOI 10.1073/pnas.1017982108.
110. Kostka and Luther, Cycling of Fe in Saltmarsh Sediments, *Biogeochemistry*. **2014.** 29(2).
111. Simpson, S. L. A rapid screening method for acid-volatile sulfide in sediments. *Environ. Tox. Chem.* **2001.** 20, 2657-2661, doi:10.1897/1551-5028(2001)020<2657:arsmfa>2.0.co;2.
112. Zhou, M. J., Diwu, Z. J., PanchukVoloshina, N. & Haugland, R. P. A stable nonfluorescent derivative of resorufin for the fluorometric determination of trace hydrogen peroxide: Applications in detecting the activity of phagocyte NADPH oxidase and other oxidases. *Anal. Biochem.* **1997.** 253, 162-168, doi:10.1006/abio.1997.2391.

Appendix A: *Environmental Science and Technology* Permissions

Copyright Clearance Center RightsLink®

Home | Create Account | Help | Live Chat

ACS Publications Most Trusted. Most Cited. Most Read.

Title: Geochemical Production of Reactive Oxygen Species From Biogeochemically Reduced Fe

Author: Sarah A. Murphy, Benson M. Solomon, Shengnan Meng, et al

Publication: Environmental Science & Technology

Publisher: American Chemical Society

Date: Apr 1, 2014

Copyright © 2014, American Chemical Society

User ID

Password

Enable Auto Login

LOGIN

Forgot Password/User ID?

If you're a copyright.com user, you can login to RightsLink using your copyright.com credentials. Already **a RightsLink user** or want to learn more?

Quick Price Estimate

Permission for this particular request is granted for print and electronic formats, and translations, at no charge. Figures and tables may be modified. Appropriate credit should be given. Please print this page for your records and provide a copy to your publisher. Requests for up to 4 figures require only this record. Five or more figures will generate a printout of additional terms and conditions. Appropriate credit should read: "Reprinted with permission from {COMPLETE REFERENCE CITATION}. Copyright {YEAR} American Chemical Society." Insert appropriate information in place of the capitalized words.

I would like to...	reuse in a Thesis/Dissertation
Requestor Type	Author (original work)
Portion	Full article
Format	Print and Electronic
Will you be translating?	No
Select your currency	USD - $
Quick Price	Click Quick Price

This service provides permission for reuse only. If you do not have a copy of the article you are using, you may copy and paste the content and reuse according to the terms of your agreement. Please be advised that obtaining the content you license is a separate transaction not involving Rightslink.

QUICK PRICE | CONTINUE

To request permission for a type of use not listed, please contact the publisher directly.

Copyright © 2014 Copyright Clearance Center, Inc. All Rights Reserved. Privacy statement.
Comments? We would like to hear from you. E-mail us at customercare@copyright.com